Research Article

OSL dating of glacial outburst flood deposits in NE Poland and their bleaching problem inferred from the landform-sediment associations and regional context

Edyta Kalińska[a] (ID), Piotr Weckwerth[a], Helena Alexanderson[b], Jan A. Piotrowski[a,c] and Wojciech Wysota[a]

[a]Nicolaus Copernicus University in Toruń, Faculty of Earth Sciences and Spatial Management, Lwowska 1, 87-100 Toruń, Poland; [b]Lund University, Department of Geology, Sölvegatan 12, 223 62 Lund, Sweden and [c]Aarhus University, Department of Geoscience, Høegh-Guldbergs Gade 2, DK-8000 Aarhus C, Denmark

Abstract

A continental-type glacial flood termed the Suwałki megafloods took place in NE Poland during the last glaciation and significantly transformed the proglacial area. This study aims, for the first time, to establish the chronology of this flood. Twenty-two sediment samples from two meltwater spillways were dated by optically stimulated luminescence. Sixteen ages from the flood megadunes are between 83 ± 11 ka and 16.9 ± 0.9 ka, whereas six ages from the outwash tracks range from 71.5 ± 9.9 ka to 20.3 ± 2.5 ka. Three dates from the uppermost part of the megadune sedimentary successions are 16.9 ± 0.9 ka, 17.9 ± 1.9 ka, and 18.8 ± 1.3 ka, and they may mark the likely true age of the Suwałki megafloods. We found no consistent relationships between the sedimentary structures and bleaching characteristics suggesting that the two are largely independent, contrary to what is typically assumed for fluvial deposits. Similarly, the transport distance from the ice margin did not exert a consistent influence on the sediment bleaching characteristics. A new hypothesis considers the stage of flooding to have a relevant impact on sediment bleaching: sediment deposited during the flood waning is well bleached and has a high potential for constraining the flood age.

Keywords: Glacial megaflood; megadune; outwash plain; Weichselian glaciation; luminescence dating; insufficient bleaching

Introduction

Massive and sudden releases of meltwater have repeatedly taken place in the history of the Earth (Carrivick and Rushmer, 2006), triggered by the melting of continental ice sheets (Clague and Evans, 2000; Kershaw et al., 2005; Murton et al., 2010; Baker, 2020) or alpine glaciers (Herget et al., 2020; Turzewski et al., 2020). The last (i.e., Weichselian) glaciation in particular generated many glacial lake outburst floods (GLOFs) (Carling et al., 2009; Margold et al., 2018; O'Connor et al., 2020; Wells et al., 2022) that left distinct landforms in the formerly glaciated areas. The timing of these events can potentially be determined by optically stimulated luminescence (OSL) dating since all these landforms carry clastic sediments with suitable grain sizes. Several GLOFs have so far been OSL dated (Zolnikov et al., 2016; Fisher, 2020; Last and Rittenour, 2021), however with various levels of success. Less successful dating highlights a risk of partial sediment bleaching (Agatova and Nepop, 2017; Herget et al., 2020; Hu et al., 2022) because of the very rapid sedimentation and turbid water typical for catastrophic fluvial events (Yang et al., 2022).

The Suwałki megafloods, which have recently been discovered in NE Poland, represent a continental GLOF-type flood with likely 2×10^6 m³/s of water released (Weckwerth et al., 2019a, 2022). This flood was originally considered to have occurred in at least two

episodes at ∼19 ka BP and probably shortly after 16 ka BP based on the bimodal orientation of scour marks (Weckwerth et al., 2019a) and the regional chronology of the ice-sheet retreat during the Weichselian glaciation in NE Poland (Marks, 2012). Nevertheless, no direct chronology has so far been provided for this event except for several OSL ages for the GLOF fans, which mainly appear to overestimate the true age (Weckwerth et al., 2024). The present study is the first attempt to constrain the age of this flood by dating the sandy deposits found in giant bedforms (megadunes) and in a meltwater spillway. We discuss a possible cause of partial sediment bleaching encountered in some samples and place our results in a wider regional chronological context. Furthermore, several sediment samples are examined in microscale for grain roundness and surface texture to better constrain their origin. Our data serve as paleoenvironmental proxies to understand the complex relationships between the sediment formation, its age, and bleaching history.

Regional setting

General framework

The study area is located in northeastern Poland close to the Lithuanian border in the heavily undulating landscape of the Eastern Suwałki Lakeland and the Augustów Plain (Fig. 1A). Large relief differences are observed here with the lowest areas at ∼30 m above sea level (asl) in the valleys and the highest area of the Wiżajny upland rising to nearly 300 m asl. The Wiżajny
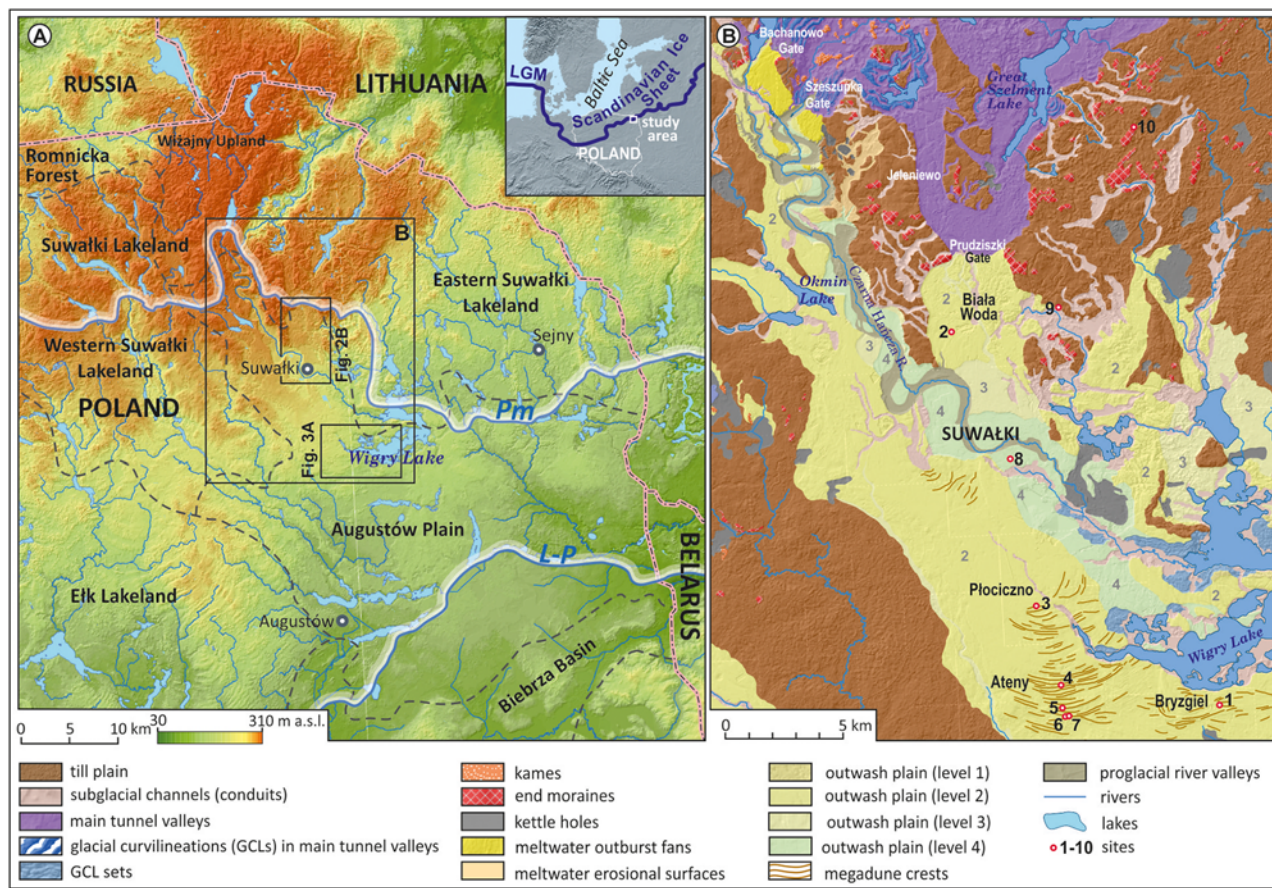
Figure 1. (A) Location of the study area in NE Poland and Europe (insert), and (B) its geomorphology. PM and L-P refer to the Pomeranian Phase and the Leszno-Poznań Phase of the last glaciation, respectively. Sites: 1 = Bryzgiel 1; 2 = Biała Woda 1-4; 3 = Płociczno 3; 4 = Płociczno 1; 5 = Ateny 2; 6 = Ateny 1; 7 = Ateny 4; 8 = Suwałki-Utrata 1; 9 = Osinki 2; 10 = Lipowo.

upland generally drops from north to south, and it borders the topographically lower Western and Eastern Suwałki lakelands and the Augustów Plain in the west, east, and south, respectively (Fig. 1). The ice-sheet and meltwater activity combined with postglacial transformation shaped this complex landscape (Smolska, 2007a, 2007b, 2008), which mainly consists of a till plain hosting end moraines, thrust and squeezed-up ridges, eskers, kettle holes, and crevasse-fill features (e.g., Kondracki and Pietkiewicz, 1967; Ber, 1974, 1982, 2000). Several subglacial meltwater valleys of different sizes hosting the Hańcza, Szeszupa, Jeleniewo, and Great Szelment lakes dissect the till plain into separate geomorphic units. The Augustów Plain lies between 130 m asl and 190 m asl and is a vast, slightly undulating outwash plain formed by proglacial meltwater activity and cut by numerous tunnel valleys (Kondracki and Pietkiewicz, 1967; Ber, 1974; Bogacki, 1976, 1980; Zieliński, 1989, 1993; Krzywicki, 2002).

Previous chronology

Age determinations are limited in the study area and derive mainly from boulder exposure dating and thermoluminescence (TL) dating studies, where mainly glacial tills and meltwater silt from the Augustów Plain were dated to between 180 ka (no error bars given; Żurek, 1990) and 23.5 ± 3.5 ka (UG-2607-09; Krzywicki, 2002). These results suggested two tills deposited during the Saalian

glaciation (Marine Oxygen Isotope Stage [MIS] 6) followed by one more till of the Świecie Stadial (MIS 3). The silt was deposited during the Grudziądz Interstadial and the Main Stadial (MIS 2) prior to the maximum ice-sheet advance (Krzywicki, 2002). Several TL ages are particularly important since they date the sediments almost directly below the sandy series of the Augustów Plain, and thus possibly constrain the age of the Augustów Plain to between 59.0 ± 8.8 to 53.7 ± 8.1 ka and 31.8 ± 4.8 to 23.5 ± 3.5 ka (see fig. 11 in Krzywicki [2002]). However, direct dating of tills by luminescence, although frequent in the last century, is highly questionable (Gemmell, 1988).

Cosmogenic [36]Cl-exposure ages have been reported for 31 erratic boulders in the Suwałki Lakeland and gave results between 28.5 ± 4.4 ka and 14.4 ± 1.0 ka, which is a time period between the advance of the ice sheet to its maximum position and the final ice melting in the Szeszupa subglacial valley, respectively (Dzierżek and Zreda, 2007), thus giving a wide age bracket for the surface sediments in the region. This is narrowed by the [10]Be ages for the Pomeranian Phase in northeastern Poland (Fig. 1A) that yielded the mean ages of 16.6 ± 1.2 ka and 14.8 ± 0.4 ka specifically in the Suwałki area (Rinterknecht et al., 2005). The most recent recalculated [10]Be surface exposure age along the Mazury Ice Stream section of the Pomeranian Phase ice-marginal belt gave a mean age of 16.4 ± 0.3 ka, including two ages from boulders located on the landforms from the maximum extent of that phase with a mean age of 16.5 ± 0.4 ka (Tylmann et al., 2022), which is consistent with the

previous inferences about the timing of the flood. The newest study determined that the flood is older than 13.2 ± 0.9 ka based on OSL dating (Weckwerth et al., 2024).

Megaflood signatures in the Suwałki area

The northern part of the Eastern Suwałki Lakeland and the Augustów Plain hosts a unique inventory of flood-related subglacial and proglacial features (Weckwerth et al., 2019a). The northern part of the Augustów outwash plain is the key junction area where floodwaters discharging through the Bachanowo, Szeszupka, Jeleniewo, and Prudziszki meltwater gates flowed through the Western and Eastern spillways, merged slightly north of Suwałki, and continued to the south (Fig. 1B). The Western Spillway was generated by a double floodwater outflow with a water depth as high as 22 m (Weckwerth et al., 2019a). A similar water depth is considered for the Eastern Spillway, however with a flow velocity higher than in the Western Spillway owing to a larger hydraulic gradient. These outflows deposited the central part of the Augustów Plain consisting of four outwash plain levels, with the first (highest) level being the oldest and the fourth (lowest) being the youngest (Figs. 1B and 2B). These outwash systems are in places dissected by subglacial channels, sometimes hosting kames, eskers, and glacial curvilineations (Fig. 1B).

The bottom part of the Western Spillway was also affected by downcutting and lateral erosion by floodwaters that generated two outburst flood terraces located below outwash plain level 2. These terraces are traceable from the Szeszupka Gate (Fig. 1B) and the Prudziszki Gate (Fig. 2B) to the town of Suwałki and Wigry Lake, and correspond to outwash plain levels 3 and 4, respectively (Weckwerth and Wysota, 2024). Further south, the extensive outwash plain level 2 hosts numerous megadunes arranged in several clusters (Figs. 1B and 3A).

Methods

Fieldwork and sampling

For the preliminary selection of fieldwork sites, a detailed light detection and ranging (LIDAR)-based digital elevation model was used. In the field, eight key sites (sand and gravel pits) were investigated: Biała Woda 1-4, Suwałki-Utrata 1, Płociczno 1 and 3, Bryzgiel 1, and Ateny 1, 2, and 4 (for location see Figs. 2B and 3A). Each site was subjected to sedimentologic investigations (Figs. 2A, 3B, and 4, Table 1) subsequently used to determine the stage of the flood (Table 2). For the determination of microscale sediment properties (Table 3), around 500 g of sand were taken parallel with the OSL sampling and transported to the Laboratory of Environmental Analyses, Nicolaus Copernicus University in Toruń, Poland for further investigation.

For the OSL sampling, we chose outwash sand that contained structures indicative of water flow conditions most favorable for effective sediment bleaching according to the recommendations by Weckwerth et al. (2013). Approximately 20-cm-long opaque PVC tubes were horizontally inserted into the sand, excavated, sealed, and transported to the laboratory in opaque bags securing full light protection. A total of 22 samples (Table 4) were shipped to the Lund Luminescence Laboratory (LLL), Lund University, Sweden for dating.

OSL sample preparation

Samples in opaque PVC tubes were opened under subdued red light conditions at the LLL. Sediment from the outer part of the tube, which may have experienced light exposure during sampling, was separated and subjected to further dose rate and water content determination. Subsequently, the inner part of the sediment in the tube was wet-sieved. The 180–250 μm fraction was used for a two-step chemical treatment. In the first step, 10% HCl was used to remove carbonates and 10% H_2O_2 to remove any organic material followed by a density separation at 2.62 g/cm³ (LST Fastfloat) to separate quartz and feldspars. In the second step, quartz extracts were treated with 40% HF for 40 min to remove remaining impurities and to etch the outer surface of the grains followed by a 10% HCl treatment to clean out any fluorides. Once the extract was dry, a magnet was used to remove magnetic grains, and then the extract was re-sieved to make sure that a strict 180–250 μm fraction was used for further measurements.

The first outer sediment part of the tube was dried at 105°C, heated to 450°C for 24 hours, mechanically ground and homogenized with warm wax, and cast in a defined geometry in the Nordic Laboratory for Luminescence Dating, Risø, Denmark. The casts were stored for at least 3 weeks to ensure equilibrium between radon and its daughter nuclides. The sediment dose rate was determined by high-resolution gamma spectrometry, and the total environmental dose rate was calculated in the DRAC online calculator (Durcan et al., 2015).

In the second outer sediment part, the weight of water per dry mass was determined to obtain the field water content and then the sample was saturated for 24 hours and dried at 105°C for 24 hours to obtain the saturated water content.

Equivalent dose measurements, calculations, and statistical treatment

Small (2 mm) single aliquots of 180–250 μm quartz were analyzed in a Risø TL/OSL reader model DA-20 (Bøtter-Jensen et al., 2010). OSL stimulation was by blue light sources (470 ± 30 nm) and detection was through 7 mm of U340 glass filter, whereas infrared stimulated luminescence (IRSL) stimulation was by infrared (IR) light (870 nm) and detection was through a Schott BG39 filter. For quartz, the first 0.8 s of the signal were integrated for the peak, followed by 0.8 s for the early background. Single aliquot regenerative (SAR) protocols (Murray and Wintle, 2000, 2003) were used, with preheat and cutheat temperatures of 260°C and 240°C, respectively, for most of the samples (Fig. 5A) except for a lower temperature combination for samples 19159 (180/180°C; Fig. 5B) and 20030 (220/180°C). A preheat plateau test and dose recovery with different preheat temperatures were used to determine the temperatures that were considered most suitable for the samples (Fig. 5A and B). The dose recovery ratio was between 0.90 ± 0.03 and 1.07 ± 0.06 (Table 5), thus being acceptable and meaning that the temperatures were correctly set up.

The laboratory dose rate was in the order of 0.16–0.20 Gy/s. Doses were calculated in the Risø Analyst 4.57 software using exponential curve fitting (Fig. 6A) and for higher doses a combination of exponential with linear curve fitting (Fig. 6B).

Aliquots were accepted when they had a test dose error of <10%, a recycling ratio within 10% of unity, and recuperation <5% of the natural. Aliquots with $D_e > 2D_0$ (i.e., close to saturation) were not rejected following Lowick et al. (2015). Nevertheless,
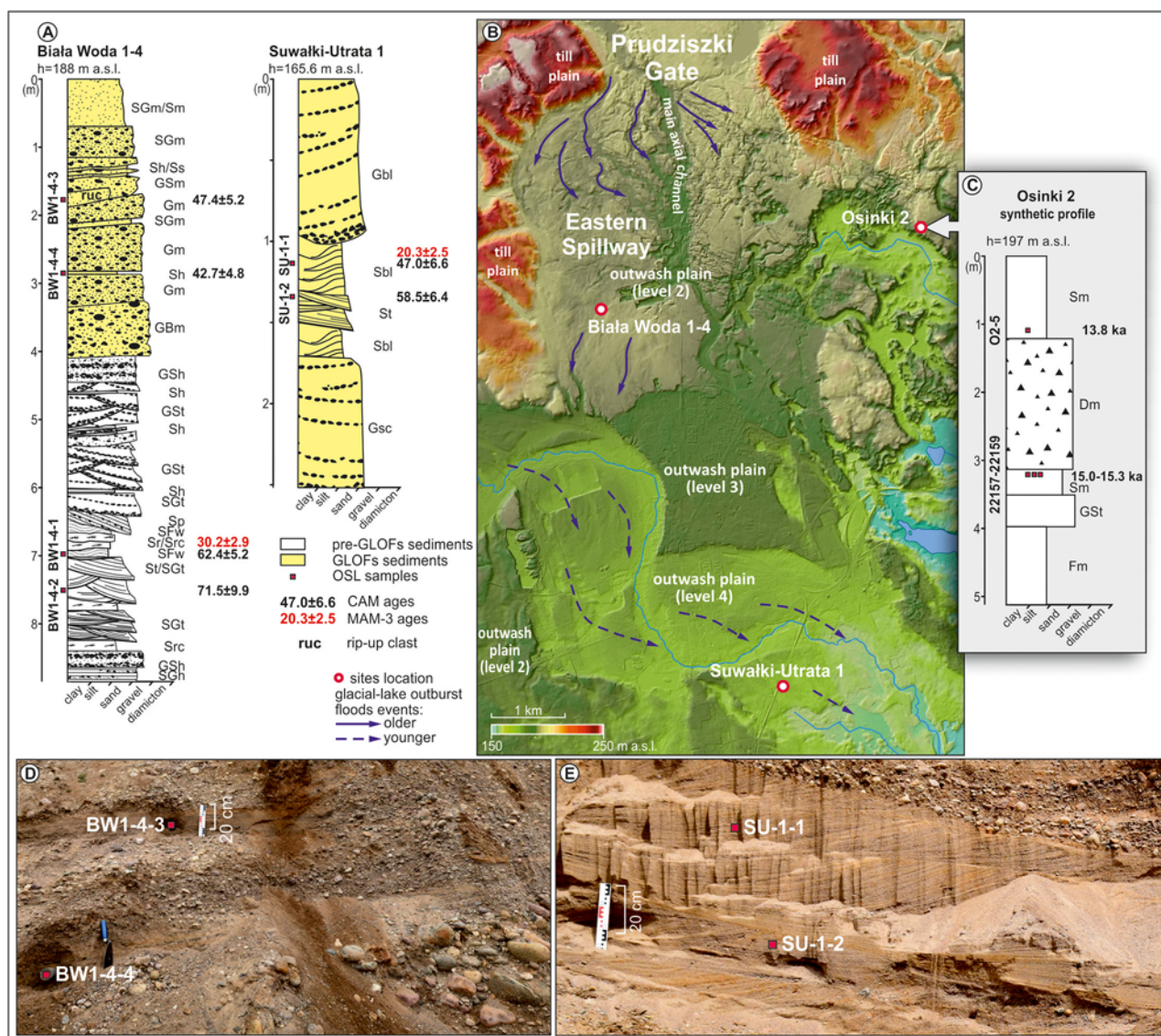
Figure 2. (A) Sediment logs from the meltwater outburst plain, (B) their detailed locations, and (D, E) examples of sedimentary structures from sampled sections. See Table 1 for details of the sedimentary structures. (C) shows the uppermost part of the Osinki 2 synthetic section. GLOFs, glacial lake outburst floods; OSL, optically stimulated luminescence; CAM, Central Age Model; MAM-3, minimum age model with three parameters.

about 35% of aliquots had to be rejected owing to apparent feldspar contamination, poor recycling, and, in some cases, test signal error.

IR-tests reveal that the mean IR/blue ratio has a wide range between 11 and 525% (samples 19154 and 20041, respectively; Table 4). For most samples, a double SAR protocol with post-IR blue stimulation was therefore used (Murray and Roberts, 1998), but for samples with only a few aliquots with an IR/blue ratio >10%, blue stimulation with an extra recycling with post-IR blue stimulation was applied to identify any aliquots with significant feldspar contamination (Duller, 2003; Murray and Wintle, 2003). Importantly, the doses do not show any significant dependence on the apparent feldspar contamination (IR/blue ratio) despite quite high values in some cases.

The mean recycling ratio, which indicates the ability to repeat a measurement, falls close to unity, which is ideal. Similarly, recuperation, which reveals the response to zero dose, is below 5% of the natural signal.

Doses for age calculation were determined using the arithmetic mean (Guérin et al., 2017) and the Central Age Model (CAM) (Galbraith et al., 1999). Ages for samples with significantly positively skewed dose distributions (Fig. 7; Supplementary material) were also calculated using the minimum age model with three parameters (MAM-3; Galbraith et al., 1999; Burow, 2021). However, MAM ages are only considered reliable for three samples (20029, 20033, and 20039), samples which had more than 30 accepted aliquots and significant probability values for the MAM age (0.12, 0.22, and 0.23, respectively). Probabilities close to zero hamper similar MAM-3 calculations for the rest of the samples. The overdispersion of the dose recovery was used for sigma b in the calculations.

Sediment textural properties

Three sediment samples (AT2-9, AT2-11, and AT2-12) from the uppermost part of the Ateny 2 section (Fig. 4) taken from
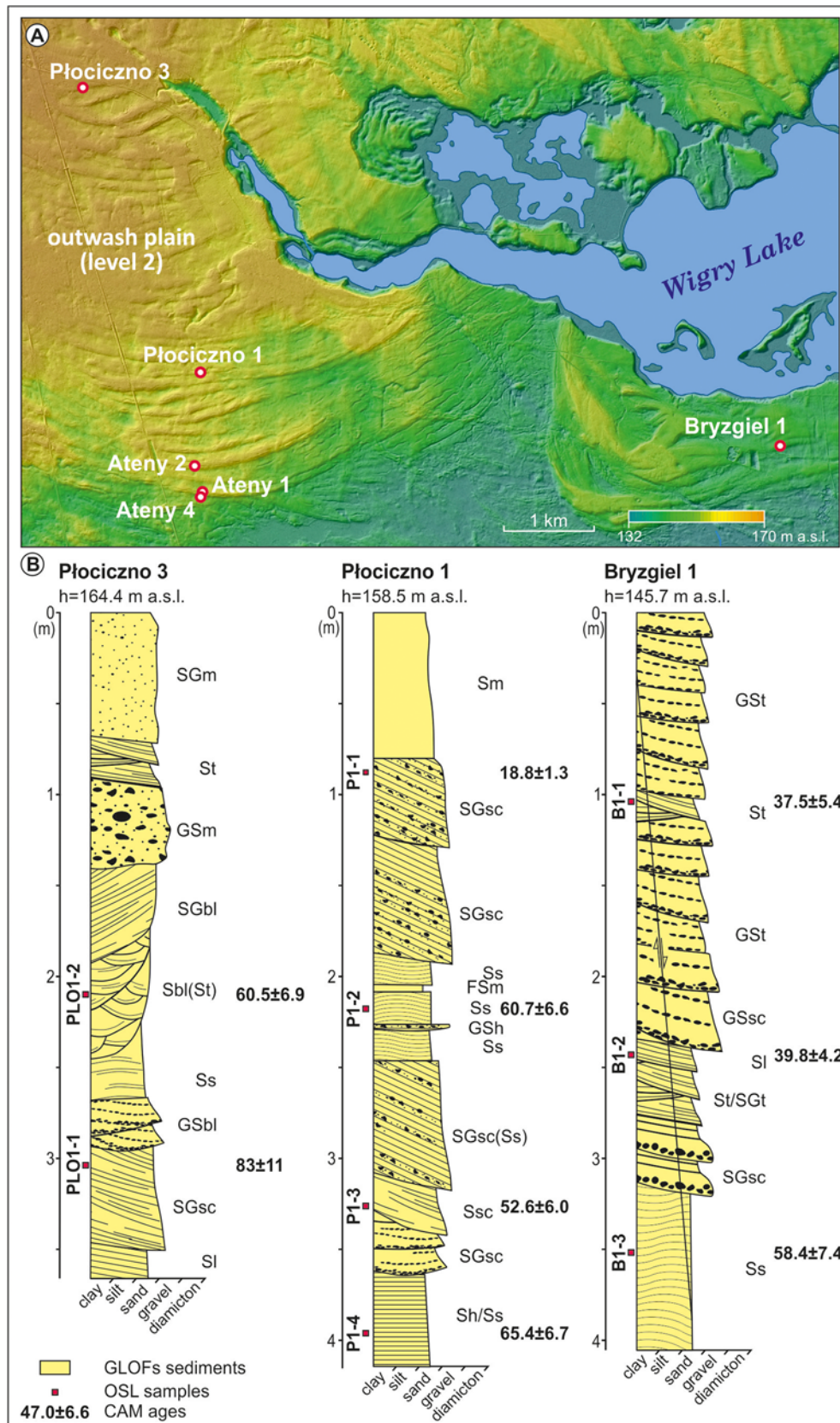
Figure 3. (A) Location of logs from the megadune field, and (B) sediment logs from the Płociczno 3 and 1 and Bryzgiel 1 sites. See Table 1 for details of the sedimentary structures. GLOFs, glacial lake outburst floods; OSL, optically stimulated luminescence; CAM, Central Age Model.

Figure 4. Sediment logs from the Ateny 1, 2, and 4 sites. See Table 1 for details of the sedimentary structures. GLOFs, glacial lake outburst floods; OSL, optically stimulated luminescence; CAM, Central Age Model; MAM-3, minimum age model with three parameters.
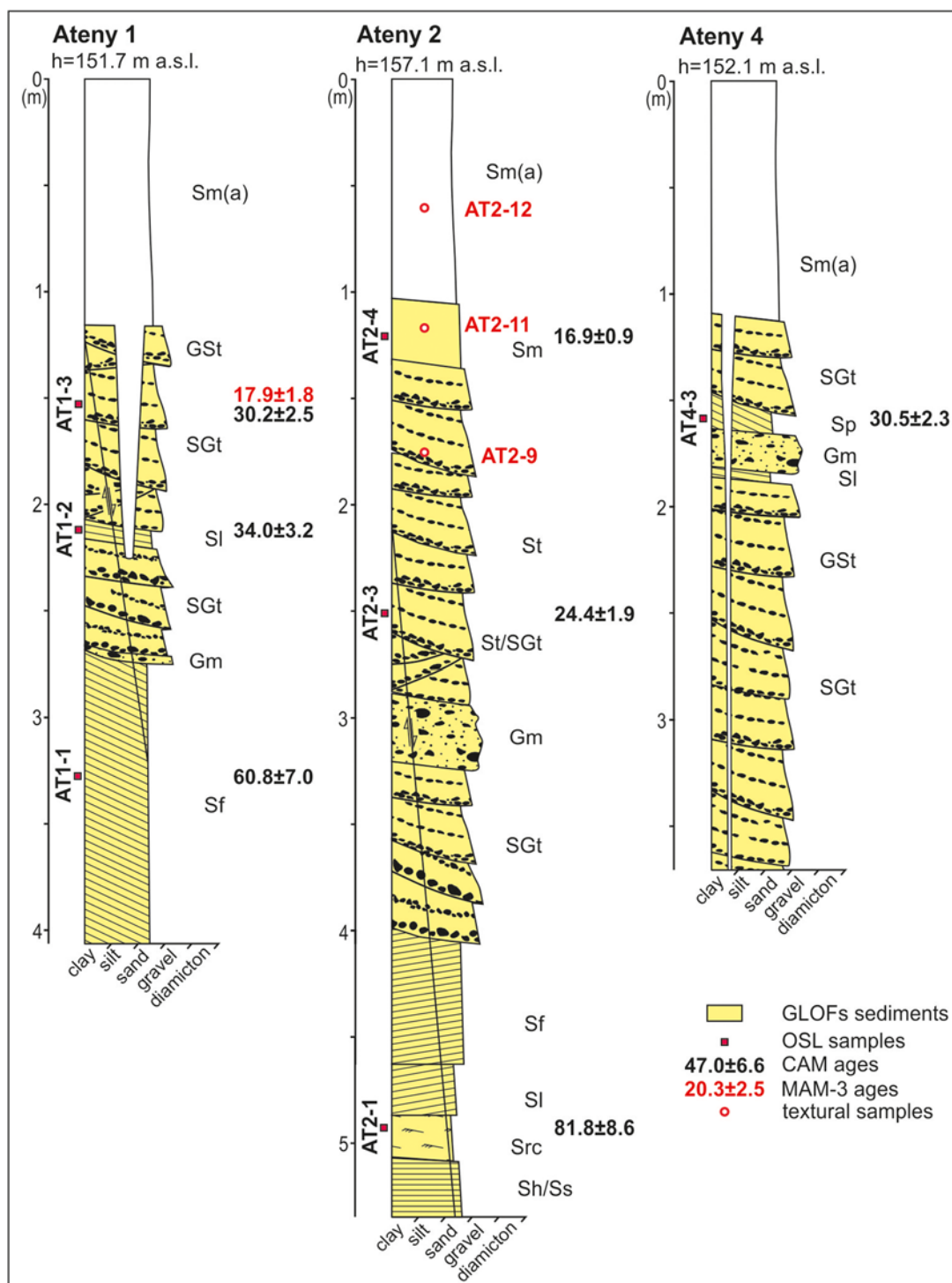
periglacially reworked massive sand lacking any diagnostic sedimentary structures were subjected to textural analysis to help constrain their origin. These sediment samples were dried at 105°C for 24 hours and dry-sieved to retain 0.5–0.8 mm and 0.8–1.0 mm sediment fractions. These fractions were treated with HCl to remove any carbonates, rinsed several times with distilled water, dried, and further viewed under a binocular microscope to determine the grain roundness and the type of grain surface following the method of Cailleux (1942) modified by Mycielska-Dowgiałło and Woronko (1998), which considers the following types of grains: aeolian-type (well-rounded and partially rounded with a matt surface; RM and EM/RM, respectively), fluvial-type (well-rounded and partially rounded with a shiny surface; EL and EM/EL, respectively), cracked with at least 30% of the grain missing (C),

Table 1. Lithofacies codes used for logging sediment characteristics (modified after Miall 1978, 1985; Lang et al. 2017a, 2017b, 2021; Winsemann et al. 2018).

Textural symbols	Sediments	Structural symbols	Stratification
D	Diamicton	m	Massive
B	Boulders	sc	Planar, trough, or sigmoidal cross stratification, symmetrically infilling the troughs
G	Gravels		
S	Sands	bl	Backset cross stratification
F	Fines (silts and clays)	f	Flaser stratification
		h	Horizontal stratification
		s	Sinusoidal cross stratification
		l	Low-angle cross stratification or subhorizontal
		t	Trough cross stratification
		p	Planar cross stratification
		i	Inclined cross stratification (large scale)
		r	Ripple cross lamination
		rc	Climbing ripple cross lamination
		w	Wavy lamination
		(a)	Aeolian

fresh with no traces of transportation (NU), and others usually with a highly weathered surface.

Results and interpretation

Geomorphology

The first set of OSL-dated sediments (samples 20029–20034; Table 4) comes from different outwash plain levels and different distances from the floodwater outlets (Fig. 1B). The Biała Woda 1-4 site is located in the proximal reach of the Eastern Spillway (Fig. 2B). This part of the Eastern Spillway is referred to as outwash plain level 2 and is characterized by at least two topographic levels with different morphologies. The lower level, where the Biała Woda 1-4 site is located, is incised by 2–4 m below the surrounding terrain at 192–193 m asl and is intersected by a system of second-rank braided channels, locally arranged in concentric arches (Weckwerth et al., 2019a, 2022). The Suwałki-Utrata 1 site occurs at 165.6 m asl and is referred to as outwash plain level 4, which lies 7–8 m below outwash plain level 2 (Fig. 2B). The differences in altitude and presumed directions of floodwater outflows (Fig. 2B) show that outwash plain level 2 predates level 4. Moreover, the occurrence of scabland-like topography with many bedforms typical of repeated high-energy scour-and-fill processes (Weckwerth et al., 2022) and the location of the Biała Woda 1-4 site around 3 km southwards of the floodwater outlet (the Prudziszki Gate) clearly distinguish this setting from the characteristics of the Suwałki-Utrata 1 site. The latter is located 18.5 km from the meltwater outlet (Bachanowo Gate) in a two-times narrower outwash track.

The second set of OSL-dated sediments (samples 19153–19159 and 20035–20043; Table 4) comes from giant bedforms (megadunes) found in two different locations and within two spatial clusters. The first cluster is located south of Suwałki, while the second is located south of Wigry Lake (Fig. 1B), and continues further southeast (Suwiński and Weckwerth, 2024). Each of them comprises ridges with parallel and semiparallel crests.

As shown by the orientation of the megadune crests within the cluster located south of Suwałki (Figs. 1B and 3A), the direction of meltwater flow was to the south. By contrast, the orientation of the megadune crests located south of Wigry Lake indicates water flow to the southwest. These morphological characteristics show different water sources and times of megadune formation. The megadune field south of Suwałki lies on outwash plain level 2, which was inundated by floodwater outflows probably at the same time through the Bachanowo, Szeszupka, and Prudziszki gates, located between 23.7 km and 14.6 km to the north.

Sediment architecture

In the proximal part of the Eastern Spillway, the pre-flood sediments are represented by a several-meters-thick series of small- and medium-scale cross-stratified sandy and gravelly lithofacies (Biała Woda 1-4 site; Fig. 2A and B). The up to 4-m-thick megaflood sedimentary succession is dominated by massive, poorly sorted, and matrix-supported boulders and cobbles with an admixture of pebbles and it contains sandy rip-up clasts (Fig. 2A and D). Within the flood sediments, pebbles and cobbles compose subhorizontal layers with crude bedding, while horizontally stratified sands form discontinuous interbeds (Fig. 2A and D).

Based on the morphological setting, the sedimentary succession at the Suwałki-Utrata 1 site represents a younger event and deposition in a more distal and confined portion of the floodwater track than at Biała Woda 1-4 (Fig. 1B). At the Suwałki-Utrata 1 site, GLOF deposits have a thickness of more than 5 m. In its middle part, large-scale gravelly scour infills occur (Gsc facies), which are capped by backset cross-stratified sands and trough cross-stratified sands (Sbl and St facies, respectively; Fig. 2A and E). In the upper part, large-scale backset cross-stratified gravels occur (Gbl).

Regarding the spatial changes in the sedimentary successions, the megadune deposits south of Suwałki show downstream-coarsening sequences from the sand-dominated sites Płociczno 3 and 1 to gravelly successions in sites Ateny 1, 2, and 4

Table 2. Sedimentary structures subjected to optically stimulated luminescence dating, their interpretation, and bleaching level.

Site	Sample ID	Environment/ landform	Obtained age (ka)	Level of bleaching	Sedimentary structure	Interpretation	GLOF stage	References
Biała Woda 1–4	BW1–4–2	Pre-GLOF/outwash	71.5 ± 9.9	Not properly bleached	St/SGt	Deposition by migrating 3D sandy or gravel dunes under conditions of subcritical flow regime	–	Miall, 1978, 1985; Carling, 2013; Hansen et al., 2020
	BW1–4–1		30.2 ± 2.9	Not properly bleached	Sr/Src	Deposition under subcritical flow from migrating current ripples and climbing ripples	–	Miall, 1978, 1985; Carling, 2013; Hansen et al., 2020
	BW1–4–4	GLOF/confined spillway	42.7 ± 4.8	Not properly bleached	Sh	Deposition under conditions of sandy upper-stage-plane bed	Rising flood	Miall, 1978, 1985; Carling, 2013
	BW1–4–3		47.4 ± 5.2	Not properly bleached	Sm (rip-up clast)	Soft-sediment clasts deposited as frozen intraclasts from suspension fall-out	Rising flood	Russell et al., 2006; Carling, 2013
Suwałki-Utrata 1	SU–1–2	GLOF/confined spillway	58.5 ± 6.4	Not properly bleached	St	Deposition by migrating 3D sandy dunes under conditions of subcritical flow regime	Rising flood	Miall, 1978, 1985; Carling, 2013; Hansen et al., 2020
	SU–1–1		20.3 ± 2.5	Not properly bleached	Sbl	Deposition by hydraulic jumps; alternatively deposits of breaking antidunes or chute-and-pool bedforms	Rising flood	Lang and Winsemann, 2013; Cartigny et al., 2014; Russell and Arnott, 2003; Duller et al., 2008; Lang and Winsemann, 2013; Cartigny et al., 2014; Lang et al., 2021
Bryzgiel 1	B1–3	Megadunes/ unconfined outwash	58.4 ± 7.4	Not properly bleached	Ss	Deposition by long- wavelength antidunes or sediment-loaded flows with high rates of suspension settling	Rising flood	Alexander et al., 2001; Fielding, 2006; Carling, 2013; Cartigny et al., 2014; Lang et al., 2017a, 2017b, 2021; Hansen et al., 2020
	B1–2		39.8 ± 4.2	Not properly bleached	Sl	Deposition by humpback dunes under transitional flow regime conditions	Rising flood	Fielding, 2006; Lang and Winsemann, 2013; Lang et al., 2017a, , 2017b
	B1–1		37.5 ± 5.4	Not properly bleached	St	Deposition by migrating 3D sandy dunes under conditions of subcritical flow regime	Waning flood	Miall, 1978, 1985; Carling, 2013; Hansen et al., 2020
Płociczno 3	PLO1–1	Megadunes/ unconfined outwash	83 ± 11	Not properly bleached	SGsc	Deposition by hydraulic jumps representing the progradational scour infills or chute-and-pool bedforms	Rising flood	Russell and Arnott, 2003; Lang and Winsemann, 2013; Cartigny et al., 2014; Lang et al., 2017a, 2017b, 2019; Slootman and Cartignyet et al., 2019; Slootman and Cartigny, 2020
	PLO1–2		60.5 ± 6.9	Not properly bleached	Sbl	Deposition by hydraulic jumps; alternatively deposits of breaking antidunes or chute-and-pool bedforms	Rising flood	Lang and Winsemann, 2013; Cartigny et al., 2014; Russell and Arnott, 2003; Duller et al., 2008; Lang and Winsemann, 2013; Cartigny et al., 2014; Lang et al., 2021

(Continued)

Table 2. (*Continued.*)

Site	Sample ID	Environment/ landform	Obtained age (ka)	Level of bleaching	Sedimentary structure	Interpretation	GLOF stage	References
Ptociczno 1	P1–4	Pre-GLOF/outwash	65.4 ± 6.7	Not properly bleached	Sh/Ss	Deposition by long- wavelength antidunes or sediment-loaded flows with high rates of suspension settling; alternatively deposition under conditions of upper-stage-plane bed	Rising flood	Alexander et al., 2001; Fielding, 2006; Carling, 2013; Cartigny et al., 2014; Lang et al., 2017a, 2017b, 2021; Hansen et al., 2020
	P1–2	Megadunes/ unconfined outwash	52.6 ± 6.0	Not properly bleached	Ssc	Deposition by hydraulic jumps representing the progradational scour infills or chute-and-pool bedforms	Rising flood	Russell and Arnott, 2003; Lang and Winsemann, 2013; Cartigny et al., 2014; Lang et al., 2017a, 2017b, 2019; Slootman et al., 2019; Slootman and Cartigny, 2020
	P1–3		60.7 ± 6.6	Not properly bleached	Ss	Deposition by long- wavelength antidunes or sediment-loaded flows with high rates of suspension settling	Rising flood	Alexander et al., 2001; Fielding, 2006; Carling, 2013; Cartigny et al., 2014; Lang et al., 2017a, 2017b, 2021; Hansen et al., 2020
	P1–4		18.8 ± 1.3	Close to proper sediment bleaching	SGsc	Deposition by hydraulic jumps representing the progradational scour infills or chute-and-pool bedforms	Waning flood	Russell and Arnott, 2003; Lang and Winsemann, 2013; Cartigny et al., 2014; Lang et al., 2017a, 2017b, 2019; Slootman et al., 2019; Slootman and Cartigny, 2020
Ateny 2	AT2–1	Megadunes/ unconfined outwash	81.8 ± 8.6	Not properly bleached	Src	Deposition under subcritical flow from climbing ripples	Rising flood	Miall, 1978, 1985; Carling, 2013; Hansen et al., 2020
	AT2–3		24.4 ± 1.9	Not properly bleached	St/SGt	Deposition by migrating 3D sandy or gravel dunes under conditions of subcritical flow regime	Waning flood	Miall, 1978, 1985; Carling, 2013; Hansen et al., 2020
	AT2–4		16.9 ± 0.9	Close to proper sediment bleaching	Sm	Rapid deposition of sands from massive suspension fall-out	Waning flood	Costa, 1983; Carling, 1987, 2013; Russell and Knudsen, 1999; Lang et al., 2017a, 2017b, 2021; Carling, 1987, 2013; Winsemann et al., 2018, Hansen et al., 2020
Ateny 1	AT1–1	Megadunes/ unconfined outwash	60.8 ± 7.0	Not properly bleached	Sf	Deposition on large-scale bed-forms from pulsing supercritical to subcritical flow	Rising flood	Fielding, 2006; Russell et al., 2006; Winsemann et al., 2018; Hansen et al., 2020;
	AT1–2		34.0 ± 3.2	Not properly bleached	Sl	Deposition by humpback dunes under transitional flow regime conditions	Waning flood	Miall, 1978, 1985; Carling, 2013; Hansen et al., 2020
	AT1–3		17.9 ± 1.8	Close to proper sediment bleaching	SGt	Deposition by migrating 3D sandy or gravel dunes under conditions of subcritical flow regime	Waning flood	Miall, 1978, 1985; Carling, 2013; Hansen et al., 2020
Ateny 4	AT4–3	Megadunes/ unconfined outwash	30.5 ± 2.3	Not properly bleached	Sp	Deposition by migrating 2D sandy dunes under conditions of subcritical flow regime	Waning flood	Miall, 1978, 1985; Carling, 2013; Hansen et al., 2020

See Table 1 for abbreviations of the sedimentary structures.
GLOF, glacial lake outburst flood.

Table 3. Results of the Cailleux ([1942]) method modified by Mycielska-Dowgiałło and Woronko ([1998]).[a]

Sample ID	0.5–0.8 mm fraction							0.8–1.0 mm fraction							Sediment origin
	Types of grains (%)														
	NU	RM	EL	EM/RM	EM/EL	C	others	NU	RM	EL	EM/RM	EM/EL	C	others	
AT2−9	8	8	10	21	6	47	0	7	4	3	20	15	50	0	Diminished aeolian factor/fluvial
AT2−11	6	5	5	24	21	38	2	3	12	3	18	13	50	1	Diminished aeolian factor/fluvial
AT2−12	1	5	2	32	27	33	1	4	10	4	33	4	45	0	Aeolian

[a]NU, fresh grains with no traces of transportation; RM, well-rounded grains with matt surface; EM/RM, partially rounded grains with matt surface; EL, well-rounded grains with shiny surface; EM/EL, partially rounded grains with shiny surface; C, cracked grains with at least 30% of grain missing; and others usually with highly weathered surface.

Table 4. Summary of doses, mean ages, modelled ages, model used, mean infrared (IR) and blue ratio, skewness, overdispersion (OD), selected probabilities (p), and number (n) of accepted and total aliquots. Probabilities close to zero are marked with a hyphen.

| Field ID	Laboratory ID Lund-	Mean dose (Gy)	Mean age (ka)	Modelled age (ka)	Model	Mean IR/blue (%)	Skewness	OD (%)	p	n acc./total
Płociczno 1–1 (P1–1)	19153	38.9 ± 2.9	19.5 ± 1.6	18.8 ± 1.3	CAM	16	1.91	26 ± 5	–	20/48
Płociczno 1–2 (P1–2)	19154	109 ± 13	70.1 ± 8.6	60.7 ± 6.6	CAM	11	1.55	49 ± 7	–	25/42
Płociczno 1–3 (P1–3)	19155	121 ± 18	63.1 ± 9.9	52.6 ± 6.0	CAM	179	3.21	54 ± 7	–	29/45
Płociczno 1–4 (P1–4)	19156	141 ± 13	70.6 ± 8.0	65.4 ± 6.7	CAM	55	1.42	34 ± 6	–	23/48
Bryzgiel 1–1 (B1–1)	19157	101 ± 19	52.0 ± 10	37.5 ± 5.4	CAM	254	2.12	68 ± 10	–	27/48
Bryzgiel 1–2 (B1–2)	19158	77.9 ± 9.7	45.1 ± 5.9	39.8 ± 4.2	CAM	55	2.65	47 ± 7	–	23/60
Bryzgiel 1–3 (B1–3)	19159	108 ± 12	70.0 ± 7.9	58.4 ± 7.4	CAM	150	0.25	60 ± 9	–	26/30
Biała Woda 1–4–1 (BW 1–4–1)	20029	114.5 ± 7.5	70.3 ± 6.4	30.2 ± 2.9	MAM-3	51	0.83	37 ± 5	0.12	41/48
Biała Woda 1–4–2 (BW 1–4–2)	20030	132 ± 17	88.0 ± 13	71.5 ± 9.9	CAM	250	1.01	57 ± 9	–	24/36
Biała Woda 1–4–3 (BW 1–4–3)	20031	92.7 ± 9.2	53.8 ± 5.9	47.4 ± 5.2	CAM	52	1.00	46 ± 7	–	23/48
Biała Woda 1–4–4 (BW 1–4–4)	20032	114 ± 14	49.2 ± 6.5	42.7 ± 4.8	CAM	92	1.56	50 ± 5	–	25/30
Suwałki-Utrata 1–1 (SU–1–1)	20033	107 ± 13	57.1 ± 8.9	20.3 ± 2.5	MAM−3	58	1.94	57 ± 8	0.22	32/36
Suwałki-Utrata 1–2 (SU–1–2)	20034	116 ± 12	67.1 ± 8.2	58.5 ± 6.4	CAM	69	1.40	48 ± 8	–	24/33
Płociczno 3–1 (PLO1–1)	20035	146 ± 17	99.0 ± 13	83.0 ± 11	CAM	62	0.67	58 ± 9	–	24/27
Płociczno 3–2 (PLO1–2)	20036	104 ± 10	67.1 ± 8.2	60.5 ± 6.9	CAM	25	1.01	41 ± 7	–	24/27
Ateny 1–1 (AT1–1)	20037	92 ± 10	70.2 ± 8.6	60.8 ± 7.0	CAM	152	1.50	50 ± 8	–	25/27
Ateny 1–2 (AT1–2)	20038	50.7 ± 4.0	36.8 ± 3.8	34.0 ± 3.2	CAM	133	1.79	33 ± 5	–	27/48
Ateny 1–3 (AT1–3)	20039	62.9 ± 4.2	32.1 ± 2.6	17.9 ± 1.8	MAM−3	107	0.89	34 ± 5	0.23	31/39
Ateny 2–1 (AT2–1)	20040	140 ± 14	91.0 ± 11	81.8 ± 8.6	CAM	181	1.62	44 ± 7	–	26/42
Ateny 2–3 (AT2–3)	20041	42.9 ± 3.0	26.2 ± 2.4	24.4 ± 1.9	CAM	525	1.90	25 ± 4	–	26/30
Ateny 2–4 (AT2–4)	20042	30.4 ± 1.6	16.9 ± 1.3	16.9 ± 0.9	CAM	34	0.59	19 ± 4	–	19/51
Ateny 4–3 (AT4–3)	20043	39.1 ± 2.8	31.3 ± 3.0	30.5 ± 2.3	CAM	31	0.94	25 ± 5	–	17/63
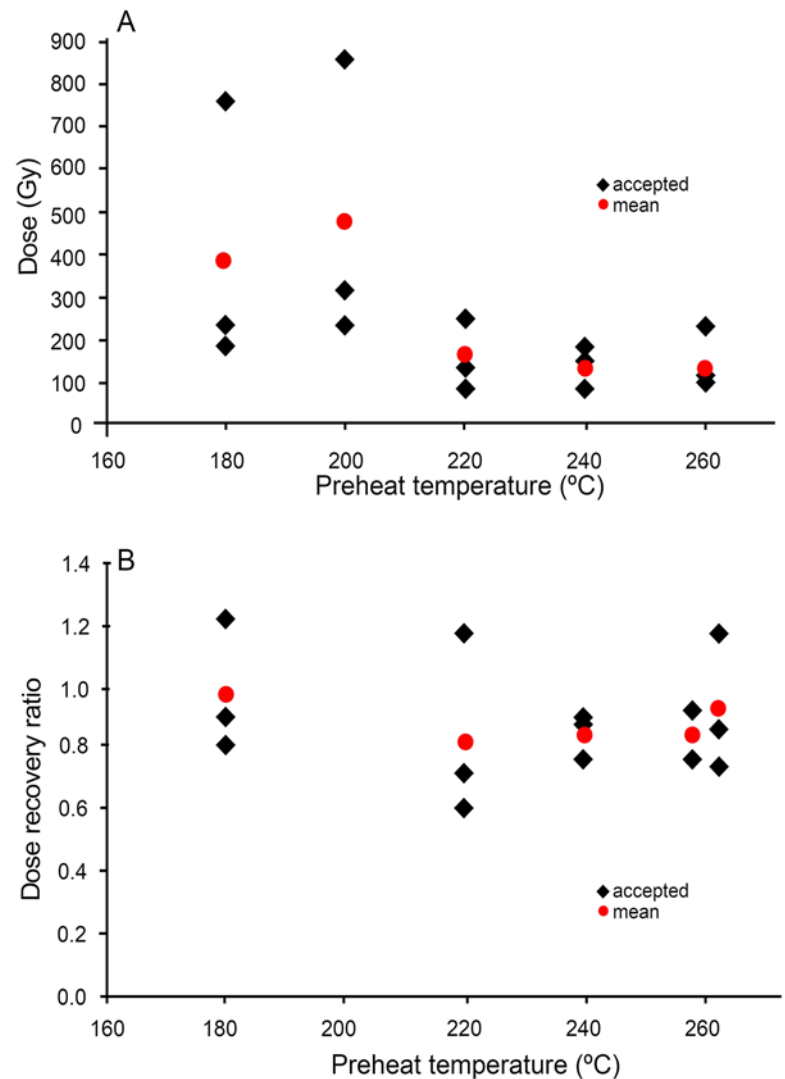
Figure 5. (A) Preheat plateau test for sample 20029 (Biała Woda 1-4-1) with scattered low temperature results and more stable doses (a plateau) for higher temperatures (≥220°C) and (B) dose recoveries with different preheat and cutheat temperatures for sample 19159 (Bryzgiel 1-3) with two sets of measurements at 260°C (preheat/cutheat combinations 260/240°C and 260/260°C, respectively).

(Figs. 3B and 4). In the proximal location (Płociczno 3 site), backset cross-stratified and scoured sands with an admixture of gravels dominate (SGbl, SGsc facies). These deposits grade into sandygravelly clinoforms at Płociczno 1 (SGi, GSi facies; Fig. 3B) and sands in the lower part of megadune successions at Ateny 1 and 2 (Fig. 4). Above the coarse-grained cross-bedded units are cosets of trough cross-stratified gravels with an admixture of sand (GSt, SGt facies). These sediments are overlain by or interbedded with massive gravels (lithofacies Gm and GSm) or trough cross-stratified sands (St). The upper parts of the megadune successions are occupied by massive gravels (Gm) or massive sands (Sm), which, in many places, are capped by massive aeolian sands (Sm(a)). Moreover, the megadune sediments are deformed by a series of normal faults dipping towards the axes of the megadune crestal depressions (sites Ateny 1 and 2 and Bryzgiel 1; Figs. 3B, 4, 8A, C, and D).

Textural properties of sediments in the upper part of the megadune succession

The uppermost, massive part of the Ateny 2 section reveals a combination of aeolian-type (well-rounded and partially rounded with a matt surface), fluvial-type (well-rounded and partially rounded with a shiny surface), and cracked grains, the latter constituting the largest share (above 50%) in the two examined sand fractions (Table 3). The topmost sample of AT2-12 (Fig. 4) is characterized by the highest share of aeolian-type grains (RM and EM/RM)—37% and 43% for the 0.5–0.8 mm and 0.8–1.0 mm fractions, respectively—whereas the proportion of aeolian-type grains in samples AT2-11 and AT2-9 (lower part of the section) does not exceed 30%. The fluvial-type grains constitute more than 26% of the share in the 0.5–0.8 mm fraction of sample AT2-11, and only 8% in the 0.8–1.0 mm fraction of sample AT2-12. Therefore, the topmost AT2-12 sample originates from aeolian deposition, whereas the aeolian input is lower in AT2-11 and AT2-9.

Luminescence characteristics

All investigated samples reveal aliquots with a clear fast signal component and fulfil the standard methodological tests as described above (Fig. 6A and B). However, occasional aliquots, especially those with high apparent feldspar contamination, also have significant medium and/or slow signal components. Growth curves

Table 5. Summary of radionuclide concentrations, total dose rates (D_r), stimulation types, and dose recovery ratios.

Laboratory ID Lund-	Radionuclide concentration $\pm$ SE			Total dose rate(D_r)	Stimulation type[a]	Dose recovery ratio
	^{238}U (ppm)	^{232}Th(ppm)	^{40}K (%)			
19153	0.85 $\pm$ 0.12	2.65 $\pm$ 0.05	1.50 $\pm$ 0.02	2.000 $\pm$ 0.075	B+IR	0.90 $\pm$ 0.03
19154	0.65 $\pm$ 0.12	2.33 $\pm$ 0.05	1.15 $\pm$ 0.02	1.554 $\pm$ 0.059	B+IR	0.96 $\pm$ 0.06
19155	0.73 $\pm$ 0.39	2.36 $\pm$ 0.10	1.49 $\pm$ 0.04	1.919 $\pm$ 0.098	IRB	1.03 $\pm$ 0.03
19156	2.32 $\pm$ 0.74	2.41 $\pm$ 0.18	1.27 $\pm$ 0.04	1.999 $\pm$ 0.138	B+IR	0.96 $\pm$ 0.01
19157	0.76 $\pm$ 0.37	2.60 $\pm$ 0.09	1.47 $\pm$ 0.03	1.957 $\pm$ 0.094	IRB	0.99 $\pm$ 0.08
19158	0.68 $\pm$ 0.14	2.30 $\pm$ 0.05	1.47 $\pm$ 0.03	1.728 $\pm$ 0.067	B+IR	1.07 $\pm$ 0.06
19159	0.97 $\pm$ 0.14	3.37 $\pm$ 0.05	1.02 $\pm$ 0.02	1.549 $\pm$ 0.059	IRB	0.97 $\pm$ 0.12
20029	1.10 $\pm$ 0.51	3.07 $\pm$ 0.13	1.36 $\pm$ 0.04	1.62 $\pm$ 0.09	IRB	0.97 $\pm$ 0.05
20030	1.00 $\pm$ 0.61	2.88 $\pm$ 0.15	1.28 $\pm$ 0.04	1.50 $\pm$ 0.10	IRB	0.95 $\pm$ 0.04
20031	1.05 $\pm$ 0.41	3.06 $\pm$ 0.10	1.45 $\pm$ 0.04	1.73 $\pm$ 0.09	IRB	0.92 $\pm$ 0.03
20032	1.54 $\pm$ 0.57	1.446 $\pm$ 0.064	1.94 $\pm$ 0.04	2.32 $\pm$ 0.12	IRB	0.94 $\pm$ 0.05
20033	1.19 $\pm$ 1.25	3.33 $\pm$ 0.23	1.65 $\pm$ 0.07	1.87 $\pm$ 0.18	IRB	1.07 $\pm$ 0.03
20034	0.96 $\pm$ 0.32	3.47 $\pm$ 0.09	1.51 $\pm$ 0.03	1.72 $\pm$ 0.08	IRB	0.90 $\pm$ 0.05
20035	1.18 $\pm$ 0.36	2.56 $\pm$ 0.09	1.17 $\pm$ 0.02	1.47 $\pm$ 0.07	IRB	0.95 $\pm$ 0.05
20036	0.88 $\pm$ 0.76	2.02 $\pm$ 0.13	1.41 $\pm$ 0.05	1.55 $\pm$ 0.12	IRB	0.91 $\pm$ 0.04
20037	1.56 $\pm$ 0.45	2.55 $\pm$ 0.11	0.97 $\pm$ 0.03	1.31 $\pm$ 0.08	IRB	0.90 $\pm$ 0.02
20038	0.71 $\pm$ 0.58	2.10 $\pm$ 0.14	1.22 $\pm$ 0.03	1.39 $\pm$ 0.09	IRB	0.93 $\pm$ 0.10
20039	0.47 $\pm$ 0.45	3.93 $\pm$ 0.11	1.85 $\pm$ 0.04	1.96 $\pm$ 0.10	IRB	1.06 $\pm$ 0.06
20040	1.69 $\pm$ 0.55	3.07 $\pm$ 0.13	1.20 $\pm$ 0.04	1.53 $\pm$ 0.09	IRB	1.00 $\pm$ 0.07
20041	0.91 $\pm$ 0.58	3.05 $\pm$ 0.10	1.46 $\pm$ 0.04	1.64 $\pm$ 0.10	IRB	1.05 $\pm$ 0.08
20042	1.19 $\pm$ 0.26	3.47 $\pm$ 0.06	1.51 $\pm$ 0.02	1.77 $\pm$ 0.07	B+IR	1.02 $\pm$ 0.02
20043	0.20 $\pm$ 0.33	1.77 $\pm$ 0.08	1.01 $\pm$ 0.02	1.25 $\pm$ 0.07	B+IR	1.02 $\pm$ 0.06

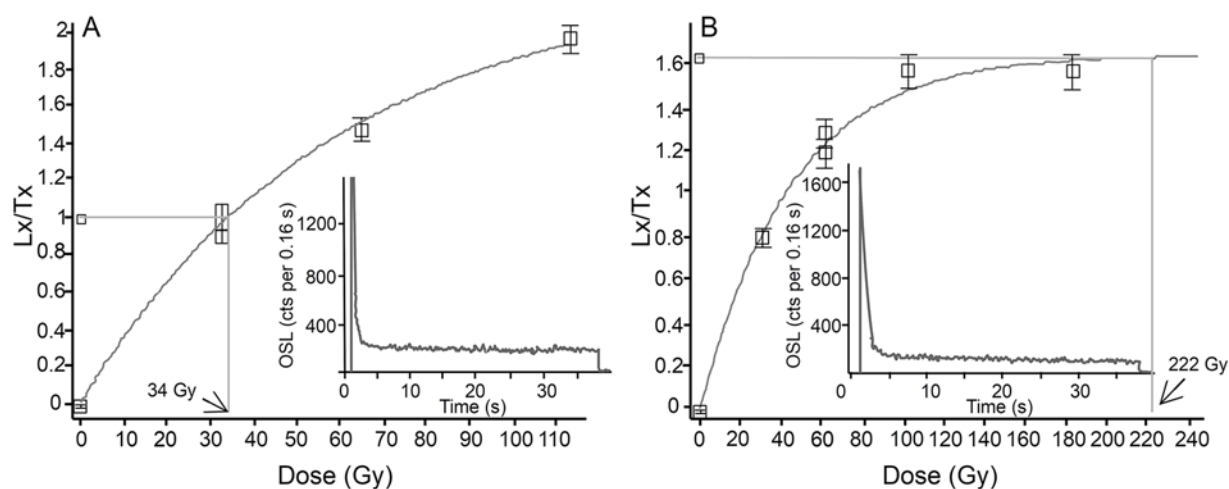[a]IRB, post-infrared blue; B+IR, blue with added infrared-test.

Figure 6. (A) Examples of optically stimulated luminescence decay and growth curves for sample 20042 (Ateny 2-4) with a steady rise of signal with dose and (B) for sample 19159 (Bryzgiel 1-3) with an aliquot that is at saturation. Decay curves in both cases show a relatively strong peak, which rapidly decays to a low background and predominance of a fast component.

reveal a steady growth of signal with dose, but most samples have at least some aliquots close to saturation. For example, sample 19159 stands out with 60% of aliquots with $D_e > 2D_0$ (Fig. 6B).

The mean D_e values of the samples show a wide spread between 146 $\pm$ 17 Gy and 30.4 $\pm$ 1.6 Gy (Table 4), whereas the total dose rate values differ between 1.25 $\pm$ 0.07 Gy/ka and 2.32 $\pm$ 0.12 Gy/ka
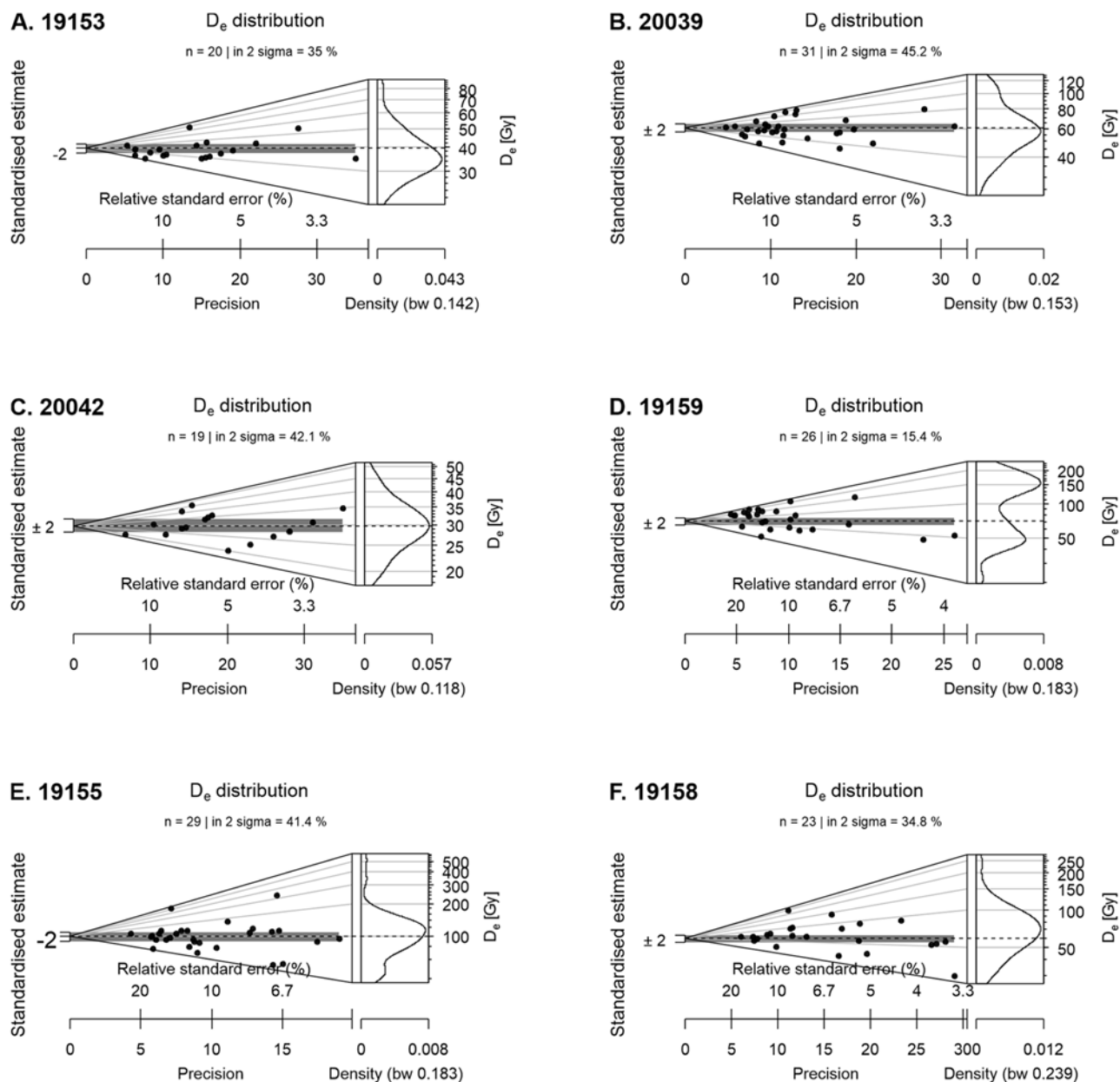
Figure 7. Examples of equivalent dose distributions (abanico plots) for the three samples revealing the youngest ages (19153, 20039, and 20042; A, B, C), sample 19159 of the lowest skewness (D), and two samples (19155 and 19158) of the highest skewness (E, F).

(Table 5). The latter is for sample 20032 and is higher than the rest of the values. The mean ages range from 16.9 ± 1.3 ka to 99 ± 13 ka, and the CAM ages are slightly younger, between 16.9 ± 0.9 ka and 83 ± 11 ka. For three samples (20029, 20033, and 20039) the MAM-3 model yielded ages between 17.9 ± 1.8 ka (20039) and 30.2 ± 2.9 ka (20029) with probability (*P*) values between 0.12 and 0.23 (Table 4), and these younger modelled ages are further discussed. Overall, the youngest obtained ages are: 16.9 ± 0.9 ka for the uppermost part of the Ateny 2 section (20042), 17.9 ± 1.8 ka for the uppermost part of Ateny 1 (20039), 18.8 ± 1.3 ka for the uppermost part of Płociczno 1 (19153), and finally 20.3 ± 2.5 ka for the uppermost part of Suwałki-Utrata 1 (20033). Overdispersion for the dated samples is considered small for the uppermost part of Ateny 1 (19%; sample 20042; Table 4) and large for the rest, reaching as high as

68% for the uppermost part of the Bryzgiel 1 section (sample 19157).

Discussion

The obtained OSL ages combined with the previous chronological study in NE Poland (Dzierżek and Zreda, 2007; Marks, 2012) allow us to consider the three youngest results between 16.9 ± 0.9 ka and 18.8 ± 1.3 ka as the most probable depositional time of the flood sediments, and this is discussed in the context of the most recent chronological data from the adjacent sediment sections. Results older than 20.3 ± 2.5 ka do not seem to mark the real time of sediment deposition, except for one (58.4 ± 7.4 ka). Furthermore, several luminescence-related issues are raised regarding the age
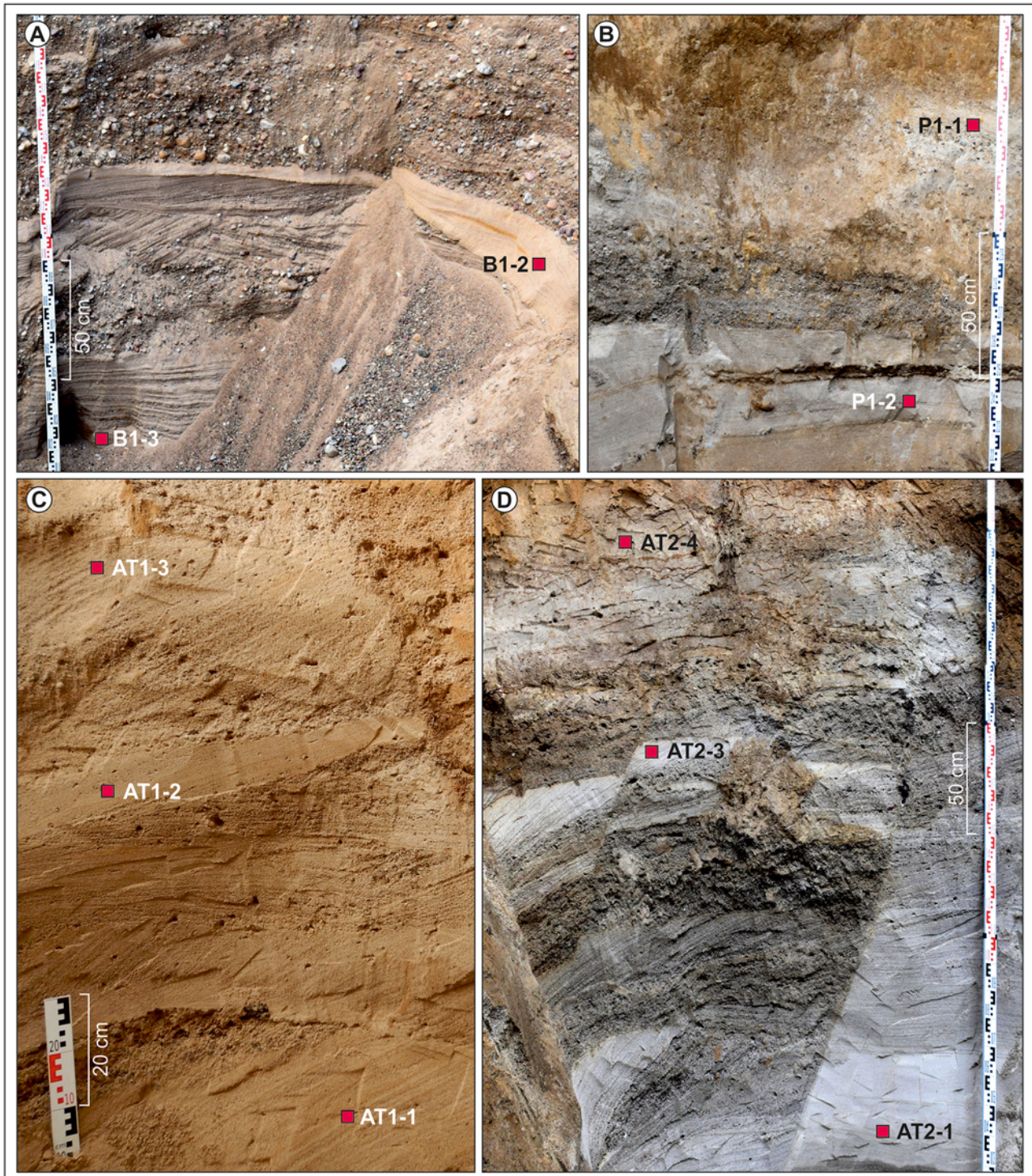
Figure 8. Examples of sedimentary structures from sections sampled in the megadune field: (A) Bryzgiel 1, (B) Płociczno 1, (C) Ateny 1, and (D) Ateny 2 sites. See Table 1 for details of the sedimentary structures.

consistencies, purity of samples, D_e distribution, and the saturation of some samples.

The luminescence context

From the age–depth perspective, the dates are more or less consistent in the investigated sections, and the Suwałki-Utrata 1,

Płociczno 3, Bryzgiel 1, and Ateny 1 and 2 sections in particular reveal older ages in the bottom parts followed by the youngest ages in the upper parts (Figs. 2A, 3B, and 4). Some age inversions occur in other investigated sections, and in particular the largest inversions of 9 ka and 8 ka are seen in the bottom parts of the Biała Woda and Płociczno 1 sections, respectively (Figs. 2A and 3B); however, they are statistically insignificant (errors within 1 sigma).
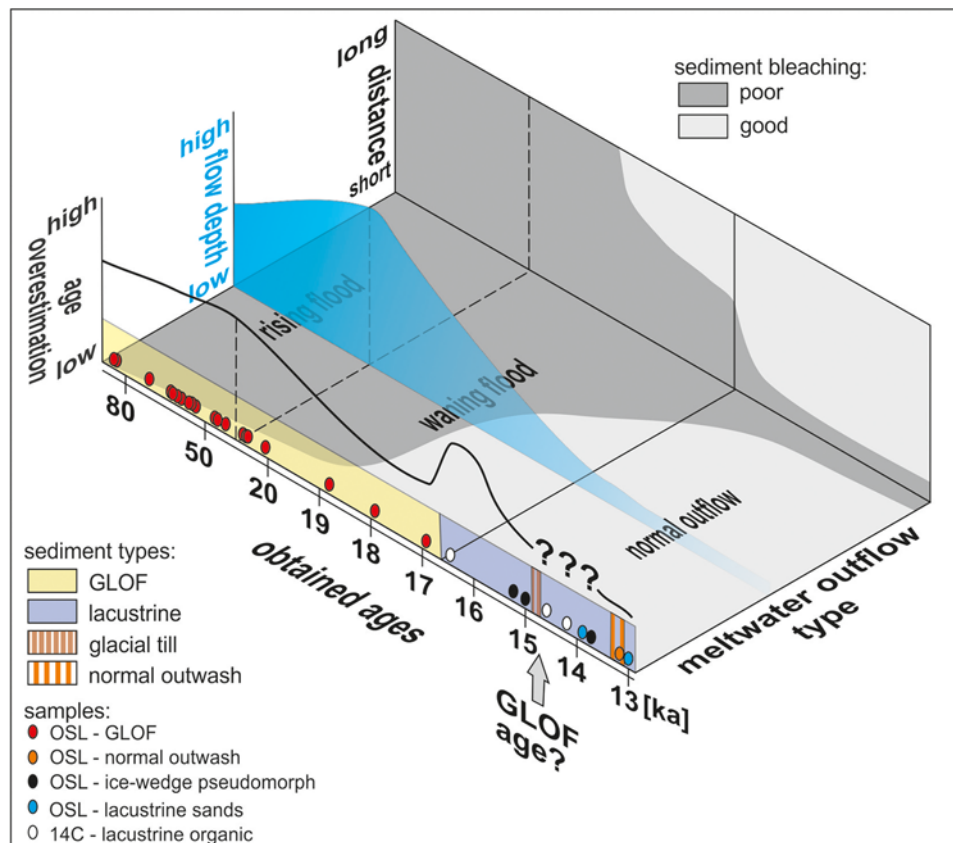
Figure 9. Relationships between the obtained ages and the environmental factors (stage of the flood and distance from the source) influencing the bleaching level of the glacial lake outburst flood sediments.

Otherwise, the dates appear in stratigraphic order, though mostly with several thousand year distances between the dates, which is larger than geologically feasible.

The IRSL/OSL ratios clearly show that only one quartz sample is relatively feldspar free (Table 4), and this clean sample comes from the Płociczno 1 site that reveals an age of 60.7 ± 6.6 ka (19154), followed by the topmost sample (19153) that marks the megaflood event at 18.8 ± 1.3 ka with a mean IR/blue ratio of 16%. In contrast, the highest feldspar-contaminated sample (20041; as high as 525%) reveals an only slightly older age of 24.4 ± 1.9 ka. With an average IRSL/OSL ratio of ~115%, most samples reveal a significant feldspar contamination, which, however, does not correspond with older or younger ages. Other studies showed that feldspar contamination may affect more significantly older samples (Tsukamoto and Rades, 2016; Long et al., 2019).

All but one (19159) sample show a significant skewness in D_e distribution (Sk ranges between 0.59 and 3.21; Fig. 7; Supplementary material). Considering a normal dose distribution for sample 19159 (skewness = 0.25; Fig. 7), the fully bleached log dose population must be represented by this sample as assumed by the commonly used statistical models of MAM-3 and MAM-4 (with four parameters) (Peng et al., 2020) and thus shows a depositional age of 58.4 ± 7.4 ka at the bottom of the Bryzgiel 1 profile, discussed later in the text. Additionally, since overdispersion is larger than 15% for multigrain samples from well-bleached sediments (Arnold and Roberts, 2009), the above suggests that most of the samples experienced only partial grain bleaching.

The MAM-3 model may help in extracting the aliquots that are best bleached, and thus closest to the true burial age of the sediments, by identifying the lowest normal dose distribution within a population (Galbraith and Roberts, 2012; Yang et al., 2022). In our study, MAM-3 gave statistically reliable results for three samples, but among them, only one age of 17.9 ± 1.8 ka (20039) from the Ateny 1 section was considered as representing the true depositional age in the context of the regional paleogeography (see below).

According to Duller (2012), saturation of the OSL signal from quartz is commonly observed and becomes more likely with the increasing age of the samples. As stated earlier, some aliquots close to saturation occur in our data set; however, a sample from the lowermost part of the Bryzgiel 1 section (19159), with an age of 58.4 ± 7.4 ka, exceeds 50% of saturated aliquots, and thus may likely be underestimating the dose (with a narrow distribution though; Fig. 7).

Timing of megadune formation and its paleogeographic context

Out of the 22 dated sediment samples, three fall into the expected time frame based on the previously obtained chronologies and inferences for the Suwałki area (e.g., Weckwerth et al., 2019a), 16.9 ± 0.9 ka, 17.9 ± 1.9 ka, and 18.8 ± 1.3 ka (samples 20042, 20039, and 19153 from the Ateny 2, Ateny 1, and Płociczno 1 profiles, respectively; Figs. 3B and 4), with no plausible explanation for older ages: These three ages overlap within a 1σ interval and point to

flood sediment deposition between 16.9 ± 0.9 ka and 18.8 ± 1.3 ka. The youngest age of 16.9 ± 0.9 ka refers to the massive topmost sands at the Ateny 2 site (Fig. 4), which are preliminarily considered either as (1) aeolian deposits, implying that dry conditions prevailed and the flooding event happened earlier, or (2) deposits from the final stage of the flood. Either way, this date provides a minimum age for megadune formation. This age is nearly 3 ka older than the aeolian dune formation in adjacent southern Lithuania, where the proximal outwash plain deposition ceased and was replaced by dune formation at 13.9–13.8 ka (Kalińska-Nartiša et al., 2015). This fact, coupled with the Cailleux analysis results (Table 3), suggests that the massive sand was deposited during the terminal flood stage when the megadune crests were finally shaped, rather than being formed by aeolian accumulation. This is further indicated by the abundance of cracked quartz grains in samples AT2-9 and AT2-11 with a modest share of aeolian-type grains, contrary to what was found in sample AT2-12 (Table 3) where grains with matt surfaces dominate (Kalińska, 2012; Kalińska-Nartiša and Nartišs, 2016). Our dates between 18.8 ± 1.3 ka and 16.9 ± 0.9 ka mark a time span of nearly 2 ka when at least two major glacial floods occurred in NE Poland (Weckwerth et al., 2019a). Regarding the local perspective of the Suwałki area and the previously obtained chronologies mentioned earlier, our OSL data set may be considered as corresponding with ^{10}Be ages of 17.2 ± 1.7 ka from the bottom part of outwash plain level 3, and 17.3 ± 1.7 ka from the till plain (see Table 1 in Tylmann et al., 2022). Furthermore, our dates are consistent with the ^{36}Cl age of 17.9 ± 1.3 ka from the top of a glacial curvilineation ridge adjacent to Hańcza Lake (Dzierżek and Zreda, 2007).

The results of our dating fall generally between the Poznań (Frankfurt) Phase and the Pomeranian Phase of the last glaciation, which have approximate ages of 19 ka and 16 ka, respectively (Marks, 2002, 2012; Tylmann et al., 2019; Marks et al., 2022), or even correspond to the Gardno Phase with its latest deglaciation age of 16.5 ± 0.6 ka (Tylmann and Uścinowicz, 2022). Importantly, the Pomeranian ice-marginal belt covers the ca. 20–15 ka period, with the eastern sector (including NE Poland) retreating later to the north than its western sector (Tylmann et al., 2022). New chronological inferences from the key Osinki site (Fig. 2C) indicate till deposition after ∼15.0–15.3 ka (massive sand in ice-wedge pseudomorphs) and before 13.8 ± 1.0 ka (massive sand atop till) in NE Poland (Wysota, W. et al., unpublished data; Figs. 2C and 9), which indicates an ice sheet advance between ∼1.6 and 3.8 earlier than the deposition of the flood sediments suggested by OSL ages obtained in this study. The flooding occurred shortly after the maximum extent of the Scandinavian Ice Sheet during the Pomeranian Phase, because the flood landforms and sediments are incised into the till plain (Fig. 1B) dated to 15.0–15.3 ka. In southern Lithuania, only a few tens of kilometers east of the study area, the age of the Baltija ice limit is considered to be around 14.7 ^{10}Be ka (Rinterknecht et al., 2008). However, as stated by Hardt and Böse (2018), this data set should be considered as being 9–15% older than the original age, i.e., around 15.3 ± 1.4 ^{10}Be ka (see the supplementary material in Hardt and Böse [2018]), because the regional ^{10}Be production rates can be significantly lower than the scaled global production rate, which results in older exposure ages. Similarly, the youngest ^{36}Cl age of 14.4 ± 1.0 ka from an erratic boulder (Dzierżek and Zreda, 2007) corresponds with the age of the Baltija ice limit if made older by 10% and it is consistent with the new chronology after W. Wysota et al. (unpublished data; Fig. 2C). Considering the above, our dates may be slightly older than the true age of the flood.

We note an occurrence of organic deposition in the adjacent Lipowo paleolake, which is believed to have taken place between 16.49 ± 0.80 cal ka BP and 13.01 ± 0.89 ka (Rychel et al., 2023; lacustrine organic matter and lacustrine sands in Fig. 9) that is after our OSL ages. However, the former date is questionable because of the sampling proximity to a diamicton likely resulting in a significant admixture of carbonates as documented by those authors (Rychel et al., 2023). Accordingly, the paleolake may have existed for a shorter time than originally suggested, that is between 14.625 ± 0.650 cal ka BP and 13.01 ± 0.89 ka (see Fig. 2C in Rychel et al. [2023] and OSL ages for lacustrine sands in Fig. 9) similar to other paleolakes in the region (Karasiewicz et al., 2024) so that the time window for the Suwałki flood would be between 15.0 ka and 14.625 ± 0.650 cal ka BP followed by some ordinary meltwater drainage at 13.2 ± 0.9 ka (Fig. 9; Weckwerth et al., 2024).

Significantly older dates and their reliability

The formation of some local "normal" outwash deposits corresponds to moderate ice-marginal fluctuations prior to the ice advance to the last glacial maximum position (LGM; Leszno Phase at 24 cal/^{10}Be/^{36}Cl ka [Marks, 2012] during the broad LGM between 29 ka and 19 ka defined by Hughes [2022] and Hughes et al. [2022]) and the R2 and the R3 runoff events of the European drainage river system (Toucanne et al., 2015; Weckwerth, 2018; Fersi et al., 2021). This outwash deposition took place in northeastern Germany at 31 ± 4 ka and 30 ± 4 ka and at the southernmost ice extent of the Weichselian glaciation (Lüthgens et al., 2020), and it also occurred repeatedly in the area of ice-marginal valleys between 30 ka and 22 ka, i.e., before the Leszno Phase in Poland (Weckwerth et al., 2013; Weckwerth and Chabowski, 2013; Weckwerth, 2018), and again between 20.1 ± 1.6 ka and 19.4 ± 2.4 ka in front of the active ice margin of the Pomeranian Phase in northeastern Germany (Lüthgens et al., 2011). Our ages between 34.0 ± 3.2 ka and 20.3 ± 2.5 ka (Ateny 1 and Suwałki-Utrata 1, respectively) seem to preliminarily correspond with the above mentioned "normal" outwash events, but considering the morphostratigraphic position of the GLOF sediments and new chronological inferences in NE Poland (i.e., the key Osinki site; Fig. 2C), the ages older than 20.3 ± 2.5 ka are substantially too old and should be disregarded in determining the age of the GLOF. One date of 58.4 ± 7.4 ka (Bryzgiel 1) in this old data set seems reliable because of a normal dose distribution (sample 19159 in Fig. 7; Lamsters et al., 2017; Kalińska et al., 2023) indicating well bleached particles; however, the dated sediment was clearly deposited by the flood (facies Ss; Fig. 3B) and we therefore consider this old age as representing bleaching during some previous event.

The issue of the reliability of our numerous evidently too old OSL ages can be addressed in different ways, for example, by comparison of the OSL results from multiple grain-size fractions from fine silt to sand (Nian et al., 2021); support by IRSL measurements on the slower bleaching feldspar (Clemmensen et al., 2018); TL measurements (Gueli et al., 2018); thermally transferred OSL (TT-OSL) (Kim et al., 2010); and independent age control (Kang et al., 2013) by comparison with existing radiocarbon ages (Thomas et al., 2003), historical records (Medialdea et al., 2014), historical maps (Quik and Wallinga, 2018), sedimentary context (Arnold and Roberts, 2011), radionuclide ages (Hu et al., 2018), electron spin resonance (Beerten et al., 2020), and many more. In our study, independent controls practically do not exist except for the sedimentary context as discussed below. Therefore, internal scrutiny of

luminescence characteristics should be applied to test whether dating is reliable or not. SAR-OSL dating has many inbuilt rigor checks for testing the reliability of measuring laboratory-given doses, such as recycling, recuperation, IR depletion ratio tests, thermal stability tests, or the dose recovery test (e.g., Trandafir et al., 2015). All these tests were performed in our study and yielded acceptable results (see "Methods" for details). Additionally, the quartz revealed a sufficient signal brightness, which suggests that the sediments have undergone many cycles of reworking and/or burial under different transport distances to improve their sensitivity. Nevertheless, our ages reveal a 66 ka spread, many dates suffer from partial grain bleaching, and the obtained ages are difficult to reconcile with the previously documented geologic history of the region. For example, two outburst events are clearly seen between the Biała Woda 1 and Suwałki-Utrata 1 sites from the hypsometric and geomorphic evidence (Fig. 2B), with the former site assigned to the older event and the latter to the younger event. Yet, the OSL ages at both sites reveal a 20 ka overlap between ∼60 ka and 40 ka with the oldest age of 71.5 ± 9.9 ka (sample 20030) in the bottom part of the Biała Woda 1 site, with no significant age difference between these sites (Fig. 2A), and with no continuous deposition. Additionally, the sediment in the top part of Biała Woda 1 yielded an age of 47.4 ± 5.2 ka (sample 20031), which corresponds within a 1σ interval with the age of 42.7 ± 4.8 ka of sand slightly below, and is younger than the lower date of 58.5 ± 6.4 ka at the Suwałki-Utrata 1 site.

Partial sediment bleaching versus environmental factors

Different environments provide various levels of daylight exposure whereby subglacial or proglacial transport at night experiences no exposure at all (Rhodes, 2011). We consider several environmental factors in the discussion of effective sediment bleaching: (1) sedimentary structures as proxies of transport mode, (2) distance from the water source, and (3) phase of flooding: rising and waning stages (Table 2, Fig. 9).

Among the sediments that yielded the youngest dates considered closest to the depositional age of the megadunes (e.g., 17.9 ± 1.8 ka [20039] in the Ateny 1 section; Figs. 4 and 8C), three types of structures appear: GSi, SGt, and Sm. Dates that are too old come from similar sedimentary structures, for example, 71.5 ± 9.9 ka (20030), 58.5 ± 6.4 ka (20034), 52.6 ± 6.0 ka (19155), 37.5 ± 5.4 ka (19157), 30.5 ± 2.3 ka (20043), and 24.4 ± 1.9 ka (20041) from St/SGt in the lowermost part of the Biała Woda 1-4 section, Suwałki-Utrata 1, Płociczno 1, Bryzgiel 1, Ateny 4, and Ateny 2 sites, respectively (Figs. 2A, 3B, 4, 8A, and 8D, Table 2). The age of 60.8 ± 7.0 ka (20037) was obtained on a sample from Si facies in the Ateny 1 section (Figs. 4 and 8C) and 47.4 ± 5.2 ka (20031) from GSm facies in Biała Woda 1-4 (Fig. 2A and D).

The fact that both ages that are close-to-true and too old come from similar sedimentary structures suggests that a megaflood setting does not ensure effective sediment bleaching, contrary to observations in ordinary rivers (Weckwerth et al., 2013). According to Weckwerth et al. (2013), ripple cross-laminated sands (Sr) accumulated on a floodplain and horizontally stratified fine-grained sand (Sh) from shallow water flows offer the best potential for effective bleaching. Also, the distal ends of bars (King et al., 2014) and top surfaces of braid-bars (Flindt et al., 2018) are expected to be completely bleached. In our study, these structures are rather scarce except for a few OSL samples obtained from Sh. Interestingly, this most promising group of samples provided the oldest ages of 65.4 ± 6.7 ka at Płociczno 1 (Fig. 3B) and 42.7 ± 4.8

ka at Biała Woda 1-4 (Fig. 2A and D). The Src facies in the lowermost part of the Ateny 2 section (Figs. 4 and 8D) is not promising either as it reveals a very old age of 81.8 ± 8.6 ka. In contrast, massive sands (Sm), revealing low proneness to sunlight bleaching because of particle mixing due to high flow turbulence and a high content of suspended particles reducing the optical transparency of the water column (Thrasher et al., 2009; Weckwerth et al., 2013), gave the youngest age of 16.9 ± 0.9 ka (Figs. 4 and 8D). Accordingly, we conclude that sedimentary structures do not help when selecting the best-bleached deposits for determining the age of a flood.

Sediments located at a distance of several kilometers from the ice-sheet margin are believed to have been sufficiently bleached (Fuchs and Owen, 2008; Alexanderson and Murray, 2012), thus potentially providing the depositional age. Therefore, the southernmost megadune sediments in our study area are predicted to be better bleached than those close to the floodwater outlet. Some of our OSL dates from different reaches of the drainage pathways are consistent with this expectation (Fig. 9), but the overall pattern is diffuse. The better-bleached sediments occur at Płociczno 1 and Ateny 1 and 2 located in the middle part of the megadune field (Figs. 1 and 3A) and representing superimposed bedforms. However, sections in the most distal megadunes (Ateny 4 and Bryzgiel 1) yielded too old ages between 39.8 ± 4.2 ka and 30.5 ± 2.3 ka. Sediments in the proximal part of the outwash plains (Biała Woda 1-4 and Suwałki-Utrata 1 sites; Figs. 1 and 2B) are not properly bleached either, but this is understandable given their proximity to the water source and short transport distance.

The stage of flooding may be deciphered from the succession of deposits, especially when the fining of sediment grain sizes marks a drop in flood energy (Costello and Walker, 1972; Marren, 2005; Carling 2013; Sobota et al., 2018; Weckwerth et al., 2019b; see Table 2). Several sites such as Płociczno 1 (Fig. 3B) and all of the Ateny sites (Fig. 4) reveal upward-fining successions, and their sediments (except for Ateny 4) seem bleached to some extent judging from the young ages obtained. The topmost part of the Ateny 4 section (sample 20043; Fig. 4) with an age of 30.5 ± 2.3 ka is similar to the uppermost part of Ateny 1 dated to 32.1 ± 2.6 ka (sample 20039 before applying the MAM-3 model), both marking the waning flood (Table 2). Since the MAM-3 model cannot be used for sample 20043 owing to a probability (p) value close to zero (Table 4) and too few measured aliquots, the age of 30.5 ± 2.3 ka cannot be recalculated as for sample 20039. In contrast to the flood termination, its rising is more difficult to trace in the sediment record mostly because of its erosive nature and sharp contacts between the pre-flood and flood sediments, such as in most of the megadune sections (Ateny 2 in Fig. 4). Assuming that the rising flood is marked by the coarse sediments, most ages obtained there are too old.

Best suited for determining the age of a flood are the deposits accumulated at the end of a flooding event (Fig. 9), with some exceptions (Table 2). This is consistent with studies on flooding in ordinary fluvial systems, where the waning flood sediments reveal a narrow age distribution reflecting a higher degree of bleaching contrary to the maximal flood stages characterized by a strong mix of different ages, resulting in a wide range of ages (Knight and Evans, 2018; Bejarano-Arias et al., 2023).

Conclusions

The first OSL dating of the sandy glacial outburst flood deposits of the Suwałki megafloods in NE Poland yielded 22 ages in a

wide time span between 83 ± 11 ka and 16.9 ± 0.9 ka. Dated were sediments from megadunes and outwash plains. All ages are considered technically reliable, because their aliquots reveal the occurrence of the fast luminescence signal component along with all fulfilled tests to adapt the analytical SAR protocol to suit each sample. However, unfavorable depositional conditions, and especially a short transport distance, give a risk of partial sediment bleaching.

The youngest ages between 18.8 ± 1.3 ka and 16.9 ± 0.9 ka were obtained from the topmost part of a megadune, and this bracket corresponds with the time of the Poznań and Gardno phases of the last glaciation in Poland. However, the most recent chronologies from the region may suggest that the Suwałki flooding events were slightly younger, given an ice advance after ~15.0 ka and onset of paleolake deposition at ~14.625 cal ka BP.

The ages older than 20.3 ka suffer from incomplete bleaching, which is seen through a broad dose distribution, large overdispersion values, and no correspondence with the regional paleogeography. Based on the occurrence of some bleached grains, the most likely environmental factor ensuring proper sediment bleaching is transport and deposition during the waning stage of the flood.

References

Agatova, A.R., Nepop, R.K., 2017. Pleistocene glaciations of the SE Altai, Russia, based on geomorphological data and absolute dating of glacial deposits in Chagan reference section. *Geochronometria* **44**, 49–65.

Alexander, J., Bridge, J.S., Cheel, R.J., Leclair, S.F., 2001. Bedforms and associated sedimentary structures formed under supercritical water flows over aggrading sand beds. *Sedimentology* **48**, 133–152.

Alexanderson, H., Murray, A.S., 2012. Problems and potential of OSL dating Weichselian and Holocene sediments in Sweden. *Quaternary Science Reviews* **44**, 37–50.

Arnold, L.J., Roberts, R.G., 2009. Stochastic modelling of multi-grain equivalent dose (D_e) distributions: implications for OSL dating of sediment mixtures. *Quaternary Geochronology* **4**, 204–230.

Arnold, L.J., Roberts, R.G., 2011. Paper I – Optically stimulated luminescence (OSL) dating of perennially frozen deposits in north-central Siberia: OSL characteristics of quartz grains and methodological considerations regarding their suitability for dating. *Boreas* **40**, 389–416.

Baker, V.R., 2020. Global megaflood paleohydrology. In: Herget, J., Fontana, A. (Eds.) *Palaeohydrology*. Springer, Cham, pp. 3–28.

Beerten, K., Verbeeck, K., Laloy, E., Vanacker, V., Vandenberghe, D., Christl, M., De Grave, J., Wouters, L., 2020. Electron spin resonance (ESR), optically stimulated luminescence (OSL) and terrestrial cosmogenic radionuclide (TCN) dating of quartz from a Plio-Pleistocene sandy formation in the Campine area, NE Belgium. *Quaternary International* **556**, 144–158.

Bejarano-Arias, I., Wees, R.M.J.V., Alexanderson, H., Janočko, J., Perić, Z.M., 2023. Testing the applicability of quartz and feldspar for luminescence dating of Pleistocene alluvial sediments in the Tatra Mountain foothills, Slovakia. *Geochronometria* **50**, 50–80.

Ber, A., 1974. Czwartorzęd Pojezierza Suwalskiego. *Biuletyn Państwowego Instytutu Geologicznego* **269**, 23–106.

Ber, A., 1982. Marginal zones and deglaciation during the north-polish glaciation in the Suwałki-Augustów Lakeland. *Biuletyn Instytutu Geologicznego* **342**, 71–89.

Ber, A., 2000. Plejstocen Polski północno-wschodniej w nawiązaniu do głębszego podłoża i obszarów sąsiednich. *Prace Państwowego Instytutu Geologicznego* **170**, 5–89.

Bogacki, M., 1976. Współczesne sandry na przedpolu Skeidararjökull (Islandia) i plejstoceńskie sandry w Polsce północno-wschodniej. *Rozprawy Uniwersytetu Warszawskiego* **99**, 1–165.

Bogacki, M., 1980. Types of outwash forms in north-east Poland. *Geographica Polonica* **43**, 25–34.

Bøtter-Jensen, L., Thomsen, K.J., Jain, M., 2010. Review of optically stimulated luminescence (OSL) instrumental developments for retrospective dosimetry. *Radiation Measurements* **45**, 253–257.

Burow, C., 2021. calc_MinDose(): Apply the (un-)logged minimum age model (MAM) after Galbraith et al. (1999) to a given De distribution. Function version 0.4.4. Luminescence: Comprehensive Luminescence Dating Data Analysis. R Package Version 0.9.11.

Cailleux, A., 1942. Les actions éoliennes périglaciaires en Europe. *Mémoires de la Société Géologique de France* **41**, 1–176.

Carling, P.A., 1987. A terminal debris-flow lobe in the northern Pennines, United Kingdom. *Earth and Environmental Science Transactions of the Royal Society of Edinburgh* **78**, 169–176.

Carling, P.A., 2013. Freshwater megaflood sedimentation: what can we learn about generic processes? *Earth-Science Reviews* **125**, 87–113.

Carling, P.A., Burr, D.M., Johnsen, T.F., Brennand, T.A., 2009. A review of open-channel megaflood depositional landforms on Earth and Mars. In: Burr, D.M., Carling, P.A., Baker, V.B. (Eds.), *Megaflooding on Earth and Mars*. Cambridge University Press, Cambridge, pp. 33–49.

Carrivick, J.L., Rushmer, E.L., 2006. Understanding high-magnitude outburst floods. *Geology Today* **22**, 60–65.

Cartigny, M.J.B., Ventra, D., Postma, G., van Den Berg, J.H., 2014. Morphodynamics and sedimentary structures of bedforms under supercritical-flow conditions: new insights from flume experiments. *Sedimentology* **61**, 712–748.

Clague, J.J., Evans, S.G., 2000. A review of catastrophic drainage of moraine-dammed lakes in British Columbia. *Quaternary Science Reviews* **19**, 1763–1783.

Clemmensen, L.B., Hougaard, I.W., Murray, A.S., Pedersen, S.S., 2018. A high-resolution sea-level proxy dated using quartz OSL from the Holocene Skagen Odde spit system, Denmark. *Boreas* **47**, 1184–1198.

Costa, J.E., 1983. Paleohydraulic reconstruction of flash-flood peaks from boulder deposits in the Colorado Front Range. *Geological Society of America Bulletin* **94**, 986–1004.

Costello, W.R., Walker, E.G., 1972. Pleistocene sedimentology, Credit River, southern Ontario: a new component of the braided river model. *Journal of Sedimentary Petrology* **42**, 389–400.

Duller, G.A.T., 2003. Distinguishing quartz and feldspar in single grain luminescence measurements. *Radiation Measurements* **37**, 161–165.

Duller, G.A.T., 2012. Improving the accuracy and precision of equivalent doses determined using the optically stimulated luminescence signal from single grains of quartz. *Radiation Measurements* **47**, 770–777.

Duller, R.A., Mountney, N.I.P., Russell, A.J., Cassidy, N.C., 2008. Architectural analysis of a volcaniclastic jökulhlaup deposit, southern Iceland: sedimentary evidence for supercritical flow. *Sedimentology* **55**, 939–964.

Durcan, J.A., King, G.E., Duller, G.A.T., 2015. DRAC: Dose Rate and Age Calculator for trapped charge dating. *Quaternary Geochronology* **28**, 54–61.

Dzierżek, J., Zreda, M., 2007. Timing and style of deglaciation of northeastern Poland from cosmogenic ^{36}Cl dating of glacial and glaciofluvial deposits. *Geological Quarterly* **51**, 203–216.

Fersi, W., Penaud, A., Wary, M., Toucanne, S., Waelbroeck, C., Rossignol, L., Eynaud, F., 2021. Imprint of seasonality changes on fluvio-glacial dynamics across Heinrich Stadial 1 (NE Atlantic Ocean). *Global and Planetary Change* **204**, 103552. https://doi.org/10.1016/j.gloplacha.2021.103552.

Fielding, C.R., 2006. Upper flow regime sheets, lenses and scour fills: extending the range of architectural elements for fluvial sediment bodies. *Sedimentary Geology* **190**, 227–240.

Fisher, T.G., 2020. Megaflooding associated with glacial Lake Agassiz. *Earth-Science Reviews* **201**, 102974. https://doi.org/10.1016/j.earscirev.2019.102974.

Flindt, A.C., Benediktsson, Í.Ö., Alexanderson, H., Möller, P., 2018. A pre-LGM sandur at Fiskarheden in NW Dalarna, central Sweden–sedimentology and glaciotectonic deformation. *Boreas* **47**, 711–737.

Fuchs, M., Owen, L.A., 2008. Luminescence dating of glacial and associated sediments: review, recommendations and future directions. *Boreas* **37**, 636–659.

Galbraith, R.F., Roberts, R.G., 2012. Statistical aspects of equivalent dose and error calculation and display in OSL dating: an overview and some recommendations. *Quaternary Geochronology* **11**, 1–27.

Galbraith, R.F., Roberts, R.G., Laslett, G.M., Yoshida, H., Olley, J.M., 1999. Optical dating of single and multiple grains of quartz from Jinmium rock shelter, northern Australia: part I, experimental design and statistical models. *Archaeometry* **2**, 339–364.

Gemmell, A.M.D., 1988. Thermoluminescence dating of glacially transported sediments: some considerations. *Quaternary Science Reviews* **7**, 277–285.

Gueli, A.M., Garro, V., Palio, O., Pasquale, S., Politi, G., Stella, G., Turco, M., 2018. TL and OSL cross-dating for Valcorrente site in Belpasso (Catania, Italy). *The European Physical Journal Plus* **133**, 542. https://doi.org/10.1140/epjp/i2018-12364-7.

Guérin, G., Christophe, C., Philippe, A., Murray, A.S., Thomsen, K.J., Tribolo, C., Urbanova, P., *et al.*, 2017. Absorbed dose, equivalent dose, measured dose rates, and implications for OSL age estimates: introducing the Average Dose Model. *Quaternary Geochronology* **41**, 163–173.

Hansen, L., Tassis, G., Høgaas, F., 2020. Sand dunes and valley fills from Preboreal glacial-lake outburst floods in south-eastern Norway – beyond the aeolian paradigm. *Sedimentology* **67**, 810–848.

Hardt, J., Böse, M., 2018. The timing of the Weichselian Pomeranian ice marginal position south of the Baltic Sea: a critical review of morphological and geochronological results. *Quaternary International* **478**, 51–58.

Herget, J., Agatova, A.R., Carling, P.A., Nepop, R.K., 2020. Altai megafloods—the temporal context. *Earth-Science Reviews* **200**, 102995. https://doi.org/10.1016/j.earscirev.2019.102995.

Hu, G., Min, R., Zhou, Y., Yang, J., Wang, Y., Wang, C., Wang, H., Wang, P., Wang, L., Fan, A., 2022. Luminescence dating of a megaflood event on a terrace of the Jinsha River, China. *Quaternary Geochronology* **70**, 101303. https://doi.org/10.1016/j.quageo.2022.101303

Hu, G., Yi, C., Zhang, J., Cao, G., Pan, B., Liu, J., Jiang, T., Yi, S., Li, D., Huang, J., 2018. Chronology of a lacustrine core from Lake Linggo Co using a combination of OSL, ^{14}C and ^{210}Pb dating: implications for the dating of lacustrine sediments from the Tibetan Plateau. *Boreas* **47**, 656–670.

Hughes, P.D., 2022. Concept and global context of the glacial landforms from the Last Glacial Maximum. In: Palacious, D., Hughes, P.D., Garcia-Ruiz, J.M., Andres, N. (Eds.), *European Glacial Landscapes: Maximum Extent of Glaciations*. Elsevier, Amsterdam, pp. 355–358.

Hughes, P.D., Palacios, D., García-Ruiz, J.M., Andrés, N., 2022. The European glacial landscapes from the Last Glacial Maximum-synthesis. In: Palacious, D., Hughes, P.D., Garcia-Ruiz, J.M., Andres, N. (Eds.), *European Glacial Landscapes: Maximum Extent of Glaciations*. Elsevier, Amsterdam, pp. 407–416.

Kalińska, E., 2012. Geological setting and sedimentary characteristics of the coversands distributed in the western part of the Blonie glaciolacustrine basin (Central Poland) – preliminary results. *Bulletin of the Geological Society of Finland* **84**, 33–44.

Kalińska, E., Weckwerth, P., Alexandeson, H., 2023. Recent advances in luminescence dating of the Late Quaternary sediments in the Baltic States, Northern Europe: a review. *Earth-Science Reviews* **236**, 104272. https://doi.org/10.1016/j.earscirev.2022.104272.

Kalińska-Nartiša, E., Nartišs, M., 2016. Sandy fan-like forms in the central-eastern Mazovian Lowland (Central Poland): textural record and chronology. *Geografiska Annaler Series A: Physical Geography* **98**, 111–127.

Kalińska-Nartiša, E., Thiel, C., Nartišs, M., Buylaert, J.P., Murray, A.S., 2015. Age and sedimentary record of inland eolian sediments in Lithuania, NE European Sand Belt. *Quaternary Research* **84**, 82–95.

Kang, S., Wang, X., Lu, Y., 2013. Quartz OSL chronology and dust accumulation rate changes since the Last Glacial at Weinan on the southeastern Chinese Loess Plateau. *Boreas* **42**, 815–829.

Karasiewicz, T., Hrynowiecka, A., Weckwerth, P., Pawłowski, D., Rzodkiewicz, M., Krzymińska, J., 2024. Palaeoecological and palaeoenvironmental responses to abrupt climate changes during the Late Vistulian: the unique archive recorded at the Osinki site (NE Poland) and its regional importance. *Quaternary International* **686**, 18–34.

Kershaw, J.A., Clague, J.J., Evans, S.G., 2005. Geomorphic and sedimentological signature of a two-phase outburst flood from moraine-dammed Queen Bess Lake, British Columbia, Canada. *Earth Surface Processes and Landforms* **30**, 1–25.

Kim, J.C., Duller, G.A.T., Roberts, H.M., Wintle, A.G., Lee, Y.I., Yi, S.B., 2010. Re-evaluation of the chronology of the palaeolithic site at Jeongokri, Korea, using OSL and TT-OSL signals from quartz. *Quaternary Geochronology* **5**, 365–370.

King, G.E., Robinson, R.A.J., Finch, A.A., 2014. Towards successful OSL sampling strategies in glacial environments: deciphering the influence of depositional processes on bleaching of modern glacial sediments from Jostedalen, Southern Norway. *Quaternary Science Reviews* **89**, 94–107.

Knight, J., Evans, M., 2018. Luminescence dating, sediment analysis, and flood dynamics on the Sabie River, South Africa. *Geomorphology* **319**, 1–14.

Kondracki, J., Pietkiewicz, S., 1967. Czwartorzęd północno-wschodniej Polski. In: Galon, R., Dylik, J. (Eds.), *Czwartorzęd Polski*. Wydawnictwo Naukowe PWN, Warszawa, pp. 207–258.

Krzywicki, T., 2002. The maximum ice sheet limit of the Vistulian Glaciation in northeastern Poland and neighbouring areas. *Geological Quarterly* **46**, 165–188.

Lamsters, K., Kalińska-Nartiša, E., Zelčs, V., Alexanderson, H., 2017. New luminescence ages reveal early to Middle Weichselian deposits in central Latvia. *Geological Quarterly* **61**, 480–490.

Lang, J., Brandes, Ch., Winsemann. J., 2017a. Erosion and deposition by supercritical density flows during channel avulsion and backfilling: field examples from coarse-grained deepwater channel-levée complexes (Sandino Forearc Basin, southern Central America). *Sedimentary Geology* **349**, 79–102.

Lang, J., Fedele, J., Hoyal, D., 2019. Bedform successions formed by submerged plane-wall jet flows. In: Lefebvre, A., Garlan, T., Winter, C. (Eds.), *Marine and River Dune Dynamics – MARID VI*. MARUM – Center for Marine Environmental Sciences, University of Bremen and SHOM, Bremen, Germany, pp. 151–156.

Lang, J., Le Heron, D.P., Van den Berg, J.H., Winsemann, J., 2021. Bedforms and sedimentary structures related to supercritical flows in glacigenic settings. *Sedimentology* **68**, 1539–1579.

Lang, J., Sievers, J., Loewer, M., Igel, J., Winsemann, J., 2017b. 3D architecture of cyclic-step and antidune deposits in glacigenic subaqueous fan and delta settings: integrating outcrop and ground-penetrating radar data. *Sedimentary Geology* **362**, 83–100.

Lang, J., Winsemann, J., 2013. Lateral and vertical facies relationships of bedforms deposited by aggrading supercritical flows: from cyclic steps to humpback dunes. *Sedimentary Geology* **296**, 36–54.

Last, G.V., Rittenour, T.M., 2021. Chronology of Missoula Flood Deposits at the Coyote Canyon Mammoth Site, Washington State, USA. *Quaternary* **4**, 1–17.

Long, H., Tsukamoto, S., Buylaert, J.P., Murray, A.S., Jain, M., Frechen, M., 2019. Late Quaternary OSL chronologies from the Qinghai Lake (NE Tibetan Plateau): inter-comparison of quartz and K-feldspar ages to assess the pre-depositional bleaching. *Quaternary Geochronology* **49**, 159–164.

Lowick, S.E., Buechi, M.W., Gaar, D., Graf, H.R., Preusser, F., 2015. Luminescence dating of Middle Pleistocene proglacial deposits from northern Switzerland: methodological aspects and stratigraphical conclusions. *Boreas* **44**, 459–482.

Lüthgens, C., Böse, M., Preusser, F., 2011. Age of the Pomeranian ice-marginal position in northeastern Germany determined by Optically Stimulated Luminescence (OSL) dating of glaciofluvial sediments. *Boreas* **40**, 598–615.

Lüthgens, C., Hardt, J., Böse, M., 2020. Proposing a new conceptual model for the reconstruction of ice dynamics in the SW sector of the Scandinavian Ice Sheet (SIS) based on the reinterpretation of published data and new evidence from optically stimulated luminescence (OSL) dating. *E&G Quaternary Science Journal* **69**, 201–223.

Margold, M., Jansen, J.D., Codilean, A.T., Preusser, F., Gurinov, A.L., Fujioka, T., Fink, D., 2018. Repeated megafloods from glacial Lake Vitim, Siberia, to the Arctic Ocean over the past 60,000 years. *Quaternary Science Reviews* **187**, 41–61.

Marks, L., 2002. Last Glacial Maximum in Poland. *Quaternary Science Reviews* **21**, 103–110.

Marks, L., 2012. Timing of the Late Vistulian (Weichselian) glacial phases in Poland. *Quaternary Science Reviews* **44**, 81–88.

Marks, L., Bitinas, A., Błaszkiewicz, M., Börner, A., Guobyte, R., Rinterknecht, V., Tylmann, K., 2022. Northern Central Europe: glacial landforms during deglaciation (18.9-14.9 ka). In: Palacious, D., Hughes, P.D., Garcia-Ruiz, J.M., Andres, N. (Eds.), *European Glacial Landscapes: Maximum Extent of Glaciations*. Elsevier, Amsterdam, pp. 95–104.

Marren, P.M., 2005. Magnitude and frequency in proglacial rivers: a geomorphological and sedimentological perspective. *Earth-Science Reviews* **70**, 203–251.

Medialdea, A., Thomsen, K.J., Murray, A.S., Benito, G., 2014. Reliability of equivalent-dose determination and age-models in the OSL dating of historical and modern palaeoflood sediments. *Quaternary Geochronology* **22**, 11–24.

Miall, A.D., 1978. Lithofacies types and vertical profile models in braided river deposits: a summary. *Fluvial Sedimentology* **5**, 597–600.

Miall, A.D., 1985. Architectural-element analysis: a new method of facies analysis applied to fluvial deposits. *Earth-Science Reviews* **22**, 261–308.

Murray, A.S., Roberts, R.G., 1998. Measurement of the equivalent dose in quartz using a regenerative-dose single-aliquot protocol. *Radiation Measurements* **29**, 503–515.

Murray, A.S., Wintle, A.G., 2000. Luminescence dating of quartz using an improved single-aliquot regenerative-dose protocol. *Radiation Measurements* **32**, 57–73.

Murray, A.S., Wintle, A.G., 2003. The single aliquot regenerative dose protocol: potential for improvements in reliability. *Radiation Measurements* **37**, 377–381.

Murton, J.B., Bateman, M.D., Dallimore, S.R., Teller, J.T., Yang, Z., 2010. Identification of Younger Dryas outburst flood path from Lake Agassiz to the Arctic Ocean. *Nature* **464**, 740–743.

Mycielska-Dowgiałło, E., Woronko, B., 1998. Analiza obtoczenia i zmatowienia powierzchni ziarn kwarcowych frakcji piaszczystej i jej wartość interpretacyjna. *Przegląd Geologiczny* **46**, 1275–1281.

Nian, X., Zhang, W., Wang, Z., Sun, Q., Chen, Z., 2021. Inter-comparison of optically stimulated luminescence (OSL) ages between different fractions of Holocene deposits from the Yangtze delta and its environmental implications. *Marine Geology* **432**, 106401. https://doi.org/10.1016/j.margeo.2020.106401.

O'Connor, J.E., Baker, V.R., Waitt, R.B., Smith, L.N., Cannon, C.M., George, D.L., Denlinger, R.P., 2020. The Missoula and Bonneville floods—a review of ice-age megafloods in the Columbia River basin. *Earth-Science Reviews* **208**, 103181. https://doi.org/10.1016/j.earscirev.2020.103181.

Peng, J., Li, B., Jacobs, Z., 2020. Modelling heterogeneously bleached single-grain equivalent dose distributions: implications for the reliability of burial dose determination. *Quaternary Geochronology* **60**, 101108. https://doi.org/10.1016/j.quageo.2020.101108.

Quik, C., Wallinga, J., 2018. Reconstructing lateral migration rates in meandering systems – a novel Bayesian approach combining optically stimulated luminescence (OSL) dating and historical maps. *Earth Surface Dynamics* **6**, 705–721.

Rhodes, E., 2011. Optically stimulated luminescence dating of sediments over the past 200,000 years. *Annual Review of Earth and Planetary Sciences* **39**, 462–488.

Rinterknecht, V.R., Bitinas, A., Clark, P.U., Raisbeck, G.M., Yiou, F., Brook, E.J., 2008. Timing of the last deglaciation in Lithuania. *Boreas* **37**, 426–433.

Rinterknecht, V.R., Marks, L., Piotrowski, J.A., Raisbeck, G.M., Yiou, F., Brook, E.J., Clark, P.U., 2005. Cosmogenic ^{10}Be ages on the Pomeranian Moraine, Poland. *Boreas* **34**, 186–191.

Russell, A.J., Knudsen, Ó., 1999. An ice-contact rhythmite (turbidite) succession deposited during the November 1996 catastrophic outburst flood (jokulhlaup), Skeidararjokull, Iceland. *Sedimentary Geology* **127**, 1–10.

Russell, A.J., Roberts, M.J., Fay, H., Marren, P.M., Cassidy, N.J., Tweed, F.S., Harris, T., 2006. Icelandic jökulhlaup impacts: implications for ice-sheet hydrology, sediment transfer and geomorphology. *Geomorphology* **75**, 33–64.

Russell, H.A.J., Arnott, R.W.C., 2003. Hydraulic-jump and hyperconcentrated-flow deposits of a glacigenic subaqueous fan: oak ridges moraine, southern Ontario, Canada. *Journal of Sedimentary Research* **73**, 887–905.

Rychel, J., Sokołowski, R.J., Sieradz, D., Hrynowiecka, A., Mirosław-Grabowska, J., Sienkiewicz, E., Niska, M., et al., 2023. Late Pleniglacial-Late Glacial climate oscillations detected in the organic lacustrine succession at the Lipowo site, north-eastern Poland. *Journal of Quaternary Science* **38**, 186–207.

Slootman, A., Cartigny, M.J.B., 2020. Cyclic steps: review and aggradation-based classification. *Earth-Science Reviews* **201**, 102949. https://doi.org/10.1016/j.earscirev.2019.102949.

Slootman, A., Cartigny, M.J.B., Vellinga, A.J., 2019. Build-up-and-fill structure: the depositional signature of strongly aggradational chute-and-pool bedforms. In: Lefebvre, A., Garlan, T., Winter, C. (Eds.), *Marine and River Dune Dynamics – MARID VI*. MARUM – Center for Marine Environmental Sciences, University of Bremen and SHOM, Bremen, Germany, pp. 213–218.

Smolska, E., 2007a. Extreme rainfalls and their impact on slopes—evaluation based on soil erosion measurements (as exemplified by the Suwałki Lakeland, Poland). *Geographia Polonica* **80**, 151–163.

Smolska, E., 2007b. Development of gullies and sediment fans in last-glacial areas on the example of the Suwałki Lakeland (NE Poland). *Catena* **71**, 122–131.

Smolska, E., 2008. Channel response to flood flows on example of the Szeszupa a river in the last-glacial area (NE Poland). *Quaestiones Geographicae* **27A**, 63–72.

Sobota, I., Weckwerth, P., Grajewski, T., Dziembowski, M., Greń, K., Nowak, M., 2018. Short-term changes in thickness and temperature of the active layer in summer in the Kaffioyra region, NW Spitsbergen, Svalbard. *Catena* **160**, 141–153.

Suwiński, M., Weckwerth, P., 2024. Large-scale bedforms in the vicinity of Serwy Lake (NE Poland): their morphometry and links to the high-energy glaciofluvial environment. *Bulletin of Geography: Physical Geography Series* **26**, 53–68.

Trandafir, O., Timar-Gabor, A., Schmidt, C., Veres, D., Anghelinu, M., Hambach, U., Simon, S., 2015. OSL dating of fine and coarse quartz from a Palaeolithic sequence on the Bistriţa Valley (Northeastern Romania). *Quaternary Geochronology* **30**, 487–492.

Thomas, P.J., Murray, A.S., Sandgren, P., 2003. Age limit and age underestimation using different OSL signals from lacustrine quartz and polymineral fine grains. *Quaternary Science Reviews* **22**, 1139–1143.

Thrasher, I.M., Mauz, B., Chiverrell, R.C., Lang, A., Thomas, G.S.P., 2009. Testing an approach to OSL dating of Late Devensian glaciofluvial sediments of the British Isles. *Journal of Quaternary Sciences* **24**, 785–801.

Toucanne, S., Soulet, G., Freslon, N., Silva Jacinto, R., Dennielou, B., Zaragosi, S., Eynaud, F., Bourillet, J.-F., Bayon, G., 2015. Millennial-scale fluctuations of the European Ice Sheet at the end of the last glacial, and their potential impact on global climate. *Quaternary Science Reviews* **123**, 113–133.

Tsukamoto, S., Rades, E.F., 2016. Performance of pulsed OSL stimulation for minimising the feldspar signal contamination in quartz samples. *Radiation Measurements* **84**, 26–33.

Turzewski, M.D., Huntington, K.W., Licht, A., Lang, K.A., 2020. Provenance and erosional impact of Quaternary megafloods through the Yarlung-Tsangpo Gorge from zircon U-Pb geochronology of flood deposits, eastern Himalaya. *Earth and Planetary Science Letters* **535**, 116113. https://doi.org/10.1016/j.epsl.2020.116113.

Tylmann, K., Rinterknecht, V.R., Woźniak, P.P., Bourlès, D., Schimmelpfennig, I., Guillou, V., Aumaître, G., Keddadouche, K., 2019. The Local Last Glacial Maximum of the southern Scandinavian Ice Sheet front: cosmogenic nuclide dating of erratics in northern Poland. *Quaternary Science Reviews* **219**, 36–46.

Tylmann, K., Rinterknecht, V.R., Woźniak, P.P., Guillour, V., ASTER Team, 2022. Asynchronous dynamics of the last Scandinavian Ice Sheet along the Pomeranian Phase ice-marginal belt: a new scenario inferred from surface exposure ^{10}Be dating. *Quaternary Science Reviews* **294**, 107755. https://doi.org/10.1016/j.quascirev.2022.107755.

Tylmann, K., Uścinowicz, S., 2022. Timing of the last deglaciation phases in the southern Baltic area inferred from Bayesian age modeling. *Quaternary Science Reviews* **287**, 107563. https://doi.org/10.1016/j.quascirev.2022.107563.

Weckwerth, P., 2018. Fluvial responses to the Weichselian ice sheet advances and retreats: implications for understanding river paleohydrology and pattern changes in Central Poland. *International Journal of Earth Sciences* **107**, 1407–1429.

Weckwerth, P., Chabowski, M., 2013. Heavy minerals as a tool to reconstruct river activity during the Weichselian glaciation (Torun Basin, Poland). *Geologos* **19**, 25–46.

Weckwerth, P., Greń, K., Sobota, I., 2019b. Controls on downstream variation in surficial sediment size of an outwash braidplain developed under high Arctic conditions (Kaffiøyra, Svalbard). *Sedimentary Geology* **387**, 75–86.

Weckwerth, P., Kalińska, E., Wysota, W., Krawiec, A., Adamczyk, A., Chabowski, M., 2022. What does transverse furrow train in scabland-like topography originate from? The unique records of upper-flow-regime bedforms of a glacial lake-outburst flood in NE Poland. *Quaternary International* **617**, 40–58.

Weckwerth, P., Kalińska, E., Wysota, W., Krawiec, A., Alexanderson, H., Chabowski, M., 2024. Evolutionary model for glacial lake-outburst fans at the ice-sheet front: development of meltwater outlets and origins of bedforms. *Geomorphology* **453**, 109125. https://doi.org/10.1016/j.geomorph.2024.109125.

Weckwerth, P., Przegietka, K.R., Chruścińska, A., Pisarska-Jamroży, M., 2013. The relation between optical bleaching and sedimentological features of fluvial deposits in the Toruń basin (Poland). *Geological Quarterly* **57**, 31–44.

Weckwerth, P., Wysota, W., 2024. Unique landscape originated by cataclysmic glacial floods at the Weichselian glaciation decline in north-eastern Poland. In: Migoń, P. (Ed.), *Landscapes and Landforms of Poland.* Springer, Cham, pp. 665–685.

Weckwerth, P., Wysota, W., Piotrowski, J.A., Adamczyk, A., Krawiec, A., Dąbrowski, M., 2019a. Late Weichselian glacier outburst floods in North-Eastern Poland: landform evidence and palaeohydraulic significance. *Earth-Science Reviews* **194**, 216–233.

Wells, G.H., Dugmore, A.J., Beach, T., Baynes, E.R.C., Sæmundsson, Þ., Luzzadder-Beach, S., 2022. Reconstructing glacial outburst floods (jökulhlaups) from geomorphology: challenges, solutions, and an enhanced interpretive framework. *Progress in Physical Geography* **46**, 398–421.

Winsemann, J., Lang, J., Polom, U., Loewer, M., Igel, J., Pollok, L., Brandes, C., 2018. Ice-marginal forced regressive deltas in glacial lake basins: geomorphology, facies variability and large-scale depositional architecture. *Boreas* **47**, 973–1002.

Yang, A., Wang, H., Liu, W., Hu, K., Liu, D., Wu, C., Hu, X., 2022. Two megafloods in the middle reach of Yarlung Tsangpo River since Last-glacial period: evidence from giant bars. *Global and Planetary Change* **208**, 103726. https://doi.org/10.1016/j.gloplacha.2021.103726.

Zieliński, T., 1989. Lithofacies and palaeoenvironmental characteristics of Suwałki outwash (Pleistocene, Northwest Poland). *Annales Societatis Geologorum Poloniae* **59**, 249–270.

Zieliński, T., 1993. Sandry Polski północno-wschodniej: osady i warunki sedymentacji. *Wydawnictwa Uniwersytetu Śląskiego* **96**, 1–95.

Zolnikov, I.D., Deev, E.V., Kotler, S.A., Rusanov, G.G., Nazarov, D.V., 2016. New results of OSL dating of Quaternary sediments in the Upper Katuň valley (Gorny Altai) and adjacent area. *Russian Geology and Geophysics* **57**, 933–943.

Żurek, S., 1990. Związek procesu zatorfienia z elementami środowiska przyrodniczego wschodniej Polski. *Roczniki Nauk Rolniczych PAN, Seria D* **220**, 1–174.